Available online at www.sciencedirect.com
SCIENCE DIRECT®
Journal of Magnetic Resonance 170 (2004) 345–371
JMR Journal of Magnetic Resonance
www.elsevier.com/locate/jmr

Formulation of Zeeman modulation as a signal filter

Robert D. Nielsen[a], Eric J. Hustedt[b], Albert H. Beth[b], Bruce H. Robinson[a,*]

[a] *Department of Chemistry, University of Washington, Seattle, WA 98195, USA*
[b] *Department of Molecular Physiology and Biophysics, Vanderbilt University, Nashville, TN 37232, USA*

Received 29 April 2004; revised 9 July 2004
Available online 19 August 2004

Abstract

The Bloch equation containing a Zeeman modulation field is solved analytically by treating the Zeeman modulation frequency as a perturbation. The absorption and dispersion signals at both 0° and 90° modulation phase are obtained. The solutions are valid to first order in the modulation frequency, but are otherwise valid for any value of modulation amplitude or microwave amplitude. A first order treatment of modulation frequency is shown to be a valid approximation over a wide range of typical experimental EPR conditions. The solutions derived from the Bloch equation suggest that the effect of over-modulation on first and second harmonic EPR spectra can be formulated as a mathematical filter that smoothes and broadens the under-modulated signal. The only adjustable filter parameter is a width that is equivalent to the applied peak-to-peak modulation amplitude. The true spin–spin and spin–lattice relaxation rates are completely determined from the under-modulated spectrum. The filters derived from the analytic solutions of the Bloch equation in the linear limit of modulation frequency are tested against numerical solutions of the Bloch equation that are valid for any modulation frequency to show their applicability. The filters are further tested using experimental EPR spectra. Experimental under-modulated spectra are mathematically filtered and compared with the experimental over-modulated spectra. The application of modulation filters to STEPR spectra is explored and limitations are discussed.

Keywords: EPR; ESR; Zeeman modulation; STEPR; DNA; BSA

1. Introduction

Zeeman field modulation originally arose in continuous wave electron paramagnetic resonance (CW EPR) as a method of signal detection. When the amplitude of the Zeeman field is modulated by a small fraction of the total field at kHz frequencies the microwave resonance signal can be detected with a lock-in detector that is frequency selective for the modulation frequency. Modulation amplitudes that are of the same magnitude as, or are larger than, the resonance line width of the EPR signal will distort the shape of the detected signal. On the other hand, larger modulation amplitudes produce stronger signals at the front end of the lock-in detector, and therefore lead to better signal to noise. In biological studies, where spin concentrations are generally low, moderate signal distortion due to over-modulation is often tolerated. When the modulation frequency is competitive with the timescale of the spin–lattice relaxation rate, the modulating field acts as a driving field for evolution of spin magnetization producing a passage effect. Under this special circumstance, the effect of modulation cannot be considered simply as a distortion of the EPR line shape, and the modulation frequency will affect the line shape even under lowest modulation amplitude conditions. Modulation can therefore be used to study the spin–lattice relaxation rate indirectly when the timescales are similar. Saturation transfer EPR (STEPR) was developed, in part, to make systematic use of modulation in this manner. For example, the rotational diffusion rates of spin-labeled proteins and

* Corresponding author. Fax: 1 206 685 8665.
E-mail address: robinson@chem.washington.edu (B.H. Robinson).

1090-7807/$ - see front matter © 2004 Elsevier Inc. All rights reserved.
doi:10.1016/j.jmr.2004.07.007

DNA have been studied by STEPR by tracking features in the EPR spectrum that are sensitive to motion-induced changes in the spin–lattice relaxation rate. As in the standard applications of modulation, the modulation amplitude is increased to obtain better signal to noise in the STEPR spectrum.

There are other EPR techniques that make use of, or are influenced by, timescale overlap of the fundamental relaxation processes with the time variation of the Zeeman field. For example, if the Zeeman field sweep rate is competitive with the relaxation rates, then ''passage'' effects are observed [1]. Another example is provided by magic angle spinning, where mechanical modulation of the sample position effectively changes the external Zeeman field orientation on a timescale competitive with spin–lattice relaxation [2]. The present paper is limited to a discussion of passage effects generated by Zeeman field modulation. STEPR is used to demonstrate the importance of modulation frequency.

Typical CW EPR spectrometers use a lock-in detector to select the signal at the modulation frequency, but are often also equipped to detect the response at twice the modulation frequency to produce a second harmonic EPR spectrum. Lock-in detectors are also phase sensitive. The component of the first or second harmonic signal that is 90° out of phase with respect to the driving modulation field (the quadrature signal) can be detected. In both experimental and theoretical studies the second harmonic quadrature absorption EPR spectrum was found empirically to have the greatest sensitivity to changes in the spin–lattice relaxation rate under STEPR conditions, and so is the principle spectrum recorded in STEPR. The first harmonic quadrature dispersion EPR spectrum exhibits similar sensitivity [3].

Early STEPR theory recognized that quadrature spectra are related to the derivatives of in-phase spectra under low modulation amplitude and low modulation frequency conditions [4]. The computational cost of including a full treatment of modulation amplitude has meant that STEPR simulations that include a complete description of the magnetic tensors and molecular motion have been restricted, for the most part, to the low modulation amplitude limit [3,5]. The equation of motion for magnetization is formulated as a stochastic Liouville equation in STEPR theory [3,6,7]. The stochastic Liouville formulation allows for the effect of molecular motion to be properly incorporated into the equation of motion. Simplifying the way in which molecular motion is treated in the equation of motion has reduced the computational cost of solving the equation of motion, and has allowed for the inclusion of modulation. One method of simplification is to restrict STEPR theory to uniaxial motion [8]. Another approach is to restrict simulation to the regime of isotropic motional narrowing of resonance lines, where the simple Bloch equation suffices. The modulating field can be easily included in the Bloch equation as a driving field, and quadrature spectra can be simulated [9]. Singel and co-workers found that numerically simulated quadrature spectra could be fit as a linear superposition from a basis set of in-phase signals and derivatives of in-phase signals, but provided no fundamental explanation for this observation. This decomposition of the quadrature signals appeared to hold over a wide range of modulation amplitudes and microwave powers [10]. The best-fit coefficients to the basis set of in-phase signals varied systematically with microwave power.

We have solved the Bloch equation with modulation by treating the modulation *frequency* as a perturbation. The small modulation frequency limit considered here is complementary to the large modulation frequency limit investigated by Kalin et al. [11]. We have obtained analytic expressions for all signals at all harmonics of modulation (absorption, dispersion, in-phase, and quadrature). The solutions are only valid up to first order in modulation frequency, but are valid for arbitrary microwave powers and modulation *amplitudes*. These solutions show exactly how the quadrature signals are composed of linear combinations of in-phase signals. The solutions also make clear what ''distortion'' due to modulation means. We find that the in-phase signals (in the linear limit of modulation frequency) can be formulated as a mathematical filter (convolution) acting on the *un-modulated* spectrum. When the filter function acts on the un-modulated spectrum it replaces each field point in the spectrum with a weighted average over all points in the spectrum that fall within a window the size of the peak-to-peak modulation amplitude. Furthermore, we have developed a second class of mathematical filters that act on the *under-modulated* signal (the signal in the limit of small modulation amplitude) to produce a signal at arbitrary modulation amplitude. The filters from this second class apply to quadrature spectra, as well. In particular, a filter exists that acts on a first harmonic under-modulated quadrature spectrum and produces the over-modulated second harmonic quadrature spectrum. The filters do not connect in-phase and quadrature signals, however. All of the filters are limited by the assumption that the modulation frequency is only included to linear order.

Our solutions to the Bloch equation provide significant insight into the relationship of the second harmonic spectrum to the corresponding first harmonic spectrum. The decomposition of the quadrature components is of particular interest for STEPR. The Bloch equation solutions are derived in the linear modulation frequency limit, which precludes significant competition of modulation frequency and spin–lattice relaxation.

However, the solutions in the low frequency regime provide a standard of what to expect from "normal" modulation effects, and therefore help make clear what a true STEPR effect is. Our results will help to tune STEPR conditions to maximize the non-trivial features in the STEPR spectrum. In a qualitative sense, the decomposition of the quadrature components into in-phase signals holds approximately in STEPR and is responsible for much of the complex structure of quadrature components observed in STEPR. Part of the observed sensitivity of the STEPR spectrum to microwave power and rotational diffusion time is because of an approximate mixing of in-phase components of the type found under normal modulation conditions. The approximate mixing coefficients are affected by both microwave power and rotational diffusion time in STEPR. This emphasizes the need for careful interpretation of the quadrature signals in STEPR. In a quantitative sense, the filters we have developed provide a tool to test whether the STEPR spectrum is actually sensitive to the interplay of modulation frequency and spin–lattice relaxation rate. For example, if a filter applied to the experimental first harmonic quadrature spectrum exactly reproduces the experimental second harmonic quadrature spectrum, then there is no unique information present in the supposedly more sensitive STEPR spectrum.

The filters we develop are tested by comparison with numerical solutions of the Bloch equation to demonstrate their validity in the linear modulation frequency regime. The concern in generalizing the filters to STEPR arises from the effect of molecular dynamics on the basic structure of the equations governing the magnetization. The technique of saturation transfer EPR relies heavily on non-trivial competition of the effect on electron resonance of the modulating field and local magnetic fields generated by molecular motion. Experimental STEPR spectra are shown to illustrate empirically the physical regime where the filter techniques fail.

The filter formulation of modulation is connected with a pre-existing approach to modulation. Hyde et al. [12] developed the technique of pseudo-modulation, which accounts for modulation heuristically. We derive the pseudo-modulation equation from first principles, thus providing a solid foundation for this technique. The filter form of modulation follows naturally from the pseudo-modulation equations and their generalization to quadrature signals.

Section 2 reviews pseudo-modulation and derives the filter form of modulation. Section 3 summarizes the absorption, dispersion, and quadrature solutions to the Bloch equations in the linear limit of modulation frequency. Section 4 tests the validity of the quadrature solutions of the Bloch equation from Section 3 by comparison with numerical solutions of the Bloch equation that are valid for any value of modulation frequency. Section 5 shows the application of the filters to experimental EPR and STEPR spectra.

2. Pseudo-modulation and the filter form of modulation

The technique of pseudo-modulation was proposed by Hyde et al. primarily for resolution enhancement of spectra acquired with low modulation frequency and amplitude [12,13]. Typically, the first harmonic absorption spectrum is obtained experimentally. By application of the equation of pseudo-modulation higher harmonics of modulation are generated, and at the same time, the noise of the original spectrum is filtered. The higher harmonics behave like derivatives of the zeroth harmonic signal. As derivatives, the higher harmonics have greater sensitivity to subtle line shape changes. The equation of pseudo-modulation is obtained by postulating that the magnetization adiabatically follows the modulation field. This postulate is justified below based upon the Bloch equation when the magnetization is expanded to first order in the modulation frequency (see Section 3 and Appendix).

The standard field configuration in an EPR experiment consists of a large static field H_0 along $\hat{z}$ and a continuous wave RF field polarized along $\hat{x}$. The absorption signal is the $\hat{y}$ component of magnetization in the rotating frame of the RF field, $\tilde{M}_y(\Delta)$. Here $\Delta = \omega - |\gamma_e| \cdot H_0$ is the field-frequency difference, where γ_e is the gyromagnetic ratio of the electron.

If a modulating field $H_m(t) = \frac{\gamma_e h_m}{2} \cdot \cos\left(\frac{2\pi}{T_m} \cdot t\right) \cdot \hat{z}$ is added to static Zeeman field, the adiabatic response of the magnetization is

$$\tilde{M}_y\left(\Delta - \frac{\gamma h_m}{2} \cdot \cos\left(\frac{2\pi}{T_m} \cdot t\right)\right).$$

The nth harmonic response at a given multiple of the frequency of modulation is obtained by the Fourier integral:

$$A_n(\Delta) = \int_0^{T_m} \tilde{M}_y\left(\Delta - \frac{\gamma h_m}{2} \cdot \cos\left(\frac{2\pi}{T_m} \cdot t\right)\right) \cdot \cos\left(\frac{2\pi \cdot n}{T_m} \cdot t\right) \cdot \frac{dt}{T_m/2}, \quad (1)$$

where T_m is the modulation period and $\omega_m = 2\pi/T_m$ is the modulation frequency. Expression (1) is equivalent to the prediction of pseudo-modulation. The adiabatic assumption is used in pseudo-modulation as follows. The absorption signal $A(\Delta) = \tilde{M}_y(\Delta)$ is written in terms of its Fourier transform representation [14].

$$A(\Delta) = \frac{1}{2\pi} \int_{-\infty}^{\infty} F(T) \cdot e^{-i \cdot \Delta \cdot T} dT, \quad (2)$$

where

$$F(T) = \int_{-\infty}^{\infty} \tilde{M}_y(\Delta) \cdot e^{i\cdot\Delta\cdot T}\, d\Delta. \tag{3}$$

To arrive at the harmonics of the modulated absorption signal the substitution $\Delta \to \Delta - \gamma h_m/2 \cdot \cos(\omega_m \cdot t)$ is made in (2) representing adiabatic response of the magnetization to the modulating field. The exponential in the Fourier transform $\exp\{i\cdot\gamma h_m/2\cdot\cos(\omega_m\cdot t)\cdot T\}$ is expanded in Bessel functions to give [15]

$$A_{mod}(\Delta) = \frac{1}{2\pi}\sum_{n=-\infty}^{\infty} (i)^n \cdot \left\{\int_{-\infty}^{\infty} F(T)\cdot J_n\left(\frac{\gamma h_m}{2}\cdot T\right) e^{-i\cdot\Delta\cdot T}\, dT\right\} e^{i\cdot n\cdot\omega_m\cdot t}.$$

The nth harmonic of ω_m is the Fourier coefficient in the sum and is therefore

$$A_n(\Delta) = \frac{1}{2^{\delta_{n,0}}\pi}\cdot (i)^n \int_{-\infty}^{\infty} F(T) J_n\left(\frac{\gamma h_m}{2}\cdot T\right) e^{-i\cdot\Delta\cdot T}\, dT. \tag{4}$$

Eq. (4) is the equation of pseudo-modulation.

The pseudo-modulation technique of Hyde et al. consists of two processes that act on the absorption signal $A(\Delta)$: (1) the signal is Fourier transformed (2) the FT is back-transformed by the pseudo-modulation Eq. (4). Analytic expressions for an over-modulated Lorentzian line shape are derivable from (4) by using the Fourier transform of a Lorentzian line shape [16]. Eq. (4) has been modified to include Gaussian broadening of the un-modulated Lorentzian, and has been evaluated both numerically and by Taylor expansion of the Bessel function in the integrand [17]. More generally, if the absorption spectrum without modulation is simulated numerically, the higher harmonics may be generated by the pseudo-modulation technique. While Hyde et al. [12] discuss the specialized application of double modulation with dual modulating fields, the most common signal in EPR spectroscopy is the first harmonic absorption signal acquired with only one modulating field. The input to the pseudo-modulation technique for a single modulation field is the un-modulated signal. To apply the pseudo-modulation equation to an experimental first harmonic signal, the signal must be acquired with low modulation amplitude so that it approximates the derivative of the un-modulated absorption. The experimental first harmonic signal is then integrated to give the input to pseudo-modulation. This adds yet another numerical integration to the pseudo-modulation process, which now totals three numerical integrations of the original spectrum to produce the output spectrum.

To remedy this situation we recast the Eq. (4) in terms of a filter function, which acts directly on the derivative spectrum. When (3) is substituted into (4) the Fourier transforms of the J_0, J_1, and J_2 Bessel functions [18] can be used to re-write Eq. (4) for the special cases of $n = 0$, 1, and 2 as:

$$\begin{aligned}
A_0(\Delta) &= \frac{1}{2\cdot\pi}\cdot\int_{-1}^{1} A\left(\Delta - \frac{\gamma h_m}{2}u\right)\cdot\frac{1}{\sqrt{1-u^2}}\, du,\\
A_1(\Delta) &= \frac{-1}{\pi}\cdot\int_{-1}^{1} A\left(\Delta - \frac{\gamma h_m}{2}u\right)\cdot\frac{u}{\sqrt{1-u^2}}\, du,\\
A_2(\Delta) &= \frac{1}{\pi}\int_{-1}^{1} A\left(\Delta - \frac{\gamma h_m}{2}u\right)\cdot\frac{(1-2u^2)}{\sqrt{1-u^2}}\, du.
\end{aligned} \tag{5}$$

The finite range in the integrals of (5) occurs because the Fourier transform of the Bessel functions with integer index are band limited. If the change of variables $u = \cos(\omega_m\cdot t)$ is made in (5) the connection with (1) is revealed. Eqs. (5) are just the 1, $\cos(\omega_m\cdot t)$, and $\cos(2\omega_m\cdot t)$ transforms of $A\left(\Delta - \frac{\gamma h_m}{2}\cos(\omega_m\cdot t)\right)$, respectively. We emphasize the pseudo-modulation formulation because it is Eq. (4) that arises directly from the Bloch equation when solving for the in-phase and quadrature components to linear order in the modulation frequency (see Section 3 and Appendix). Eqs. (5) still suffer the defect that they require the absorption signal without modulation, $A(\Delta)$, to generate a modulated spectrum. It is desirable to have the filter expressed in terms of the low modulation amplitude first harmonic signal as an input because this is experimentally common. Also, the filters in (5) have a sharp dependence at the "turning" points of the modulation, because of $\sqrt{1-u^2}$ in the denominator. Both of these undesirable features of (5) may be removed from the first and second harmonic cases as follows.The expression (5) for first harmonic is integrated by parts to give:

$$A_1(\Delta) = \frac{\gamma h_m}{2\pi}\int_{-1}^{1}\left\{\frac{\partial}{\partial\Delta}A\left(\Delta - \frac{\gamma h_m}{2}u\right)\right\}\cdot\sqrt{1-u^2}\, du. \tag{6}$$

In practice Eq. (6) is applied as:

$$A_1(\Delta) = \frac{2}{\pi\cdot\gamma h_m}\cdot\int_{-\gamma h_m/2}^{\gamma h_m/2}\left\{\frac{\partial}{\partial\Delta}A(\Delta - u)\right\}\cdot\sqrt{\left(\frac{\gamma h_m}{2}\right)^2 - u^2}\, du. \tag{7}$$

The filter (7) acts upon the first harmonic absorption in the low modulation limit ($\partial A/\partial\Delta$). The filter process depends only on h_m; all other details of the line shape enter through the input ($\partial A/\partial\Delta$).

When the second harmonic expression from (5) is integrated by parts:

$$A_2(\Delta) = \frac{-1}{2\pi}\cdot\gamma h_m\int_{-1}^{1}\left\{\frac{\partial}{\partial\Delta}A\left(\Delta - \frac{\gamma h_m}{2}u\right)\right\}\cdot u\cdot\sqrt{1-u^2}\, du. \tag{8}$$

Another integration by parts gives:

$$A_2(\Delta) = \frac{\gamma h_{\mathrm{m}}^2}{12\pi}\int_{-1}^{1}\left\{\frac{\partial^2}{\partial\Delta^2}A\left(\Delta-\frac{\gamma h_{\mathrm{m}}}{2}u\right)\right\}\cdot\left(\sqrt{1-u^2}\right)^3\mathrm{d}u. \tag{9}$$

Consequently, the modulated second harmonic absorption signal is generated by a filter (9) acting upon the low modulation limit of the second harmonic signal ($\partial^2 A/\partial\Delta^2$). The expressions (6), (8), and (9) are all of direct utility because they expresses the modulated spectrum in terms of the low modulation limit (derivative spectrum). These filters will be demonstrated below by their action on simulated and experimental spectra. Fig. 1 summarizes the action of the filters.

The pseudo-modulation technique (and the novel variant shown here) is an incomplete description of modulation. First, only the absorption signal is treated; as yet, it is unclear how to treat dispersion. Second, the adiabatic approximation means that the magnetization follows the modulating field instantaneously, as if it were a static addition to the Zeeman field. This means that no phase-lag between the magnetization response and the modulating filed can develop. Therefore, pseudo-modulation cannot predict the quadrature absorption or dispersion signals. Both of these issues are addressed and solved when Eq. (4) is derived from first principles below from the Bloch equation in the low modulation frequency limit. It will be demonstrated that the filters in Fig. 1 can be generalized not only to the in-phase dispersion signal, but they can be extended all quadrature signals, as well.

3. Absorption and dispersion signals, in-phase and quadrature, from the Bloch equation

The details of the derivation of the in-phase and quadrature signals from the Bloch equation are given in the Appendix. All of the results derived in the Appendix are obtained by a formal Taylor expansion of the magnetization in the modulation frequency variable. Only terms up to linear order in the modulation frequency are retained. Section 4 provides examples that illustrate when the linear expansion becomes invalid (see the discussion of Figs. 11 and 12). We summarize

$$\begin{array}{lll}
\dfrac{\partial A}{\partial\Delta} & \xrightarrow{f_{11}} \quad A_1 & f_{11} = \sqrt{1-u^2} \\
\downarrow f_{12} \quad \searrow f_{12} & & f_{12} = u\cdot\sqrt{1-u^2} \\
\dfrac{\partial^2 A}{\partial\Delta^2} & \xrightarrow{f_{22}} \quad A_2 & f_{22} = \left(\sqrt{1-u^2}\right)^3
\end{array}$$

Fig. 1. Relation of the first and second harmonic absorption signals to derivative spectra through the action of filters f_{11} from the Eq. (6), f_{12} from the Eq. (8), and f_{22} from the Eq. (9). The filter variable is denoted by u, and is applied as described in the text.

the expressions for in-phase and quadrature signals from the Appendix here. We then connect the resulting expressions with the pseudo-modulation Eq. (4).The in-phase absorption and dispersion are given by:

$$A_n(\Delta) = \gamma h_1\cdot M_0\cdot(\mathrm{i})^n\frac{R_2}{R_2'}\int_0^\infty \mathrm{e}^{-R_2'\cdot T}J_n\left(\frac{\gamma h_{\mathrm{m}}}{2}\cdot T\right)\times\begin{pmatrix}\cos(\Delta\cdot T)\\ \mathrm{i}\cdot\sin(\Delta\cdot T)\end{pmatrix}_{n\,\mathrm{odd}}^{n\,\mathrm{even}}\mathrm{d}T \tag{10}$$

and

$$D_n(\Delta) = \gamma h_1\cdot M_0\cdot(\mathrm{i})^n\int_0^\infty \mathrm{e}^{-R_2'\cdot T}J_n\left(\frac{\gamma h_{\mathrm{m}}}{2}\cdot T\right)\times\begin{pmatrix}\sin(\Delta\cdot T)\\ -\mathrm{i}\cdot\cos(\Delta\cdot T)\end{pmatrix}_{n\,\mathrm{odd}}^{n\,\mathrm{even}}\mathrm{d}T, \tag{11}$$

where h_1 is the amplitude of the RF field. M_0 is the equilibrium induced magnetization in the absence of the RF field, and $R_2' = R_2\cdot\sqrt{1+\frac{(\gamma h_1)^2}{R_1\cdot R_2}}$. The connection of (10) and (11) with pseudo-modulation is discussed below.

The absorption and dispersion quadrature signals (denoted with a prime) are given in terms of the in-phase signals by:

$$A_n'(\Delta) = -\frac{n\cdot\omega_{\mathrm{m}}}{2}\cdot\left(\frac{(1+K)}{2}\cdot\frac{\partial}{\partial\Delta}D_n(\Delta)-\frac{(1-K)}{2R_2}\cdot A_n(\Delta)\right) \tag{12}$$

and

$$D_n'(\Delta) = \frac{n\cdot\omega_{\mathrm{m}}}{2}\cdot\left(\frac{(1+K)}{2}\cdot\left(\left(\frac{R_2'}{R_2}\right)^2\frac{\partial}{\partial\Delta}A_n(\Delta)\right)-\frac{(1-K)}{2}\cdot\left(\frac{1}{R_2}D_n(\Delta)+\frac{1}{(R_2)^2}\int_{-\infty}^{\Delta}A_n(\Delta)\,\mathrm{d}\Delta\right)\right) \tag{13}$$

or

$$D_n'(\Delta) = \frac{n\cdot\omega_{\mathrm{m}}}{2}\cdot\left(\frac{(1+K)}{2}\left(\left(\frac{R_2'}{R_2}\right)^2\frac{\partial}{\partial\Delta}A_n(\Delta)\right)-\frac{(1-K)}{2}\left(\frac{1}{R_2}D_n(\Delta)-\frac{1}{(R_2)^2}\cdot\frac{\gamma_e h_{\mathrm{m}}}{2\cdot n}\cdot(A_{n+1}(\Delta)-A_{n-1}(\Delta))\right)\right),$$

where ω_{m} is the modulation frequency and

$$K = \left(1-\left(\frac{\gamma h_1}{R_1}\right)^2\right)\Big/\left(1+\frac{R_1}{R_2}\cdot\left(\frac{\gamma h_1}{R_1}\right)^2\right) \equiv \frac{1-S_0}{1+(R_1/R_2)\cdot S_0},\quad S_0 = \left(\frac{\gamma h_1}{R_1}\right)^2.$$

The Bessel function in the integrand of Eq. (10) is either even or odd depending upon whether the index n is an even or odd integer. The latter fact allows the integration range in (10) to be re-written symmetrically from $-\infty$ to ∞. When Eq. (10) is re-written in the form of Eq. (4) the value of $F(T)$ can be identified as:

$$F(T) = \gamma h_1 \cdot M_0 \cdot \frac{R_2}{R_2'} e^{-R_2' \cdot |T|},$$

the Fourier transform of a Lorentizian line shape [16]. Therefore, the solution of the Bloch equation under linear modulation frequency (10) is the prediction of the pseudo-modulation Eq. (4), assuming the un-modulated absorption line shape is a Lorentizian.

The integration range in the expression for the in-phase dispersion signal (11) cannot be written symmetrically because the parity of the Bessel function is opposite that of the trigonometric function. It should also be noted that the expression for the absorption signal (11) contains a factor R_2/R_2', which is important for saturating values of the microwave amplitude. An important similarity that the dispersion formula shares with absorption is that the effect of modulation can be expressed by the same filter that was developed for absorption above (see Fig. 1).

The quadrature signals (12) and (13) are composed of the in-phase signals (10) and (11). That is, the quadrature signals are composed of the in-phase signals regardless of the value of modulation amplitude. The differentiation and integration operations that act on the in-phase signals in (12) and (13) commute with the operation of the filters (6), (8), and (9). The filters (6), (8), and (9) are therefore applicable to the quadrature signals, as well. Eqs. (10) and (11) can be evaluated analytically using known expressions for the integrals over Bessel functions, and are compared with numerical solutions of the Bloch equation elsewhere [16]. We focus here on Eqs. (12) and (13) by solving the Bloch equation numerically for the in-phase and quadrature signals. The numerically generated in-phase signals are used to generate the quadrature signals according to (12) and (13), and the results are compared with the numerically simulated quadrature solutions.

There are two approaches to solving the Bloch equation that we indicate here. In both approaches the magnetization is expressed as a Fourier series and the Bloch equation is rewritten as an infinite set of coupled simultaneous equations for the Fourier coefficients (see Appendix). The solution of the Bloch equation amounts to a diagonalization of an infinite matrix. One method of solution is to truncate this infinite matrix at the Nth harmonic followed by standard finite-matrix diagonalization. We call this procedure direct diagonalization. As shown in the Appendix, direct diagonalization can be carried out numerically, or analytically. The $N \to \infty$ limit of the analytic expressions gives Eqs. (10)–(13). An alternative approach is to formulate the infinite set of equations as a matrix continued fraction, and to solve by convergents. This method, developed elsewhere, is summarized in the Appendix [9].

4. Illustration of quadrature signal composition and the action of modulation filters using numerical evaluation of the Bloch equation

The previous sections established the connection of the Bloch equation with pseudo-modulation and its generalization to dispersion and quadrature signals. We now test the filters (6), (8), and (9) and quadrature composition Eqs. (12) and (13) through comparison with numerical evaluation of the Bloch equation. The two methods used to simulate the Bloch equation numerically are the continued fraction convergent approach and direct diagonalization. Numerical implementation of the continued fraction convergent approach is detailed in Robinson et al [9]. The simulation routine used here was written by Robinson et al., and includes the effect of modulation frequency to all orders. Unless indicated otherwise the convergents were truncated at the 10th harmonic for simulations shown in this section. The direct diagonalization approach is straightforward. The matrix manipulation environment Matlab was used, and matrix inverses were computed with the built-in inversion routines [19]. When direct diagonalization is referred to below the numerical solution of (A.5) is meant. Eq. (A.5) treats the modulation frequency as a first order perturbation. The form of the matrix solution could easily be modified to include higher order modulation frequency effects. This is not done here because we wish to compare with the analytic equations derived under the linear modulation frequency assumption with numerical direct diagonalization. We rely upon the numerical continued fraction solution of Robinson et al. to provide accurate line shapes with arbitrary modulation frequency.

4.1. Test of quadrature composition

The expressions for the quadrature signals (12) and (13) are tested in Figs. 2–5. Quadrature signals are constructed as linear combinations of in-phase signals, and are compared to the numerically generated quadrature signals. The coefficients of the linear combination of in-phase signals in the quadrature spectrum are governed by the degree of saturation according to the value of the factor $S_0 = (\gamma h_1/R_1)^2$ (see Section 3). When $S_0 \approx 1$, the two in-phase signals that contribute to the total quadrature signal are of comparable amplitude (see (12), for example). The figures below all have parameters such that $S_0 \approx 1$, unless otherwise indicated.

Fig. 2 shows the first harmonic in-phase absorption and dispersion signals (left panels, top and bottom) and quadrature absorption and dispersion signals (right panels, top and bottom). The modulation amplitude is eight times the intrinsic line width. The modulation frequency is 10 kHz. The solid lines (in all panels) were simulated numerically using the direct diagonalization method described above. The "dots" were simulated

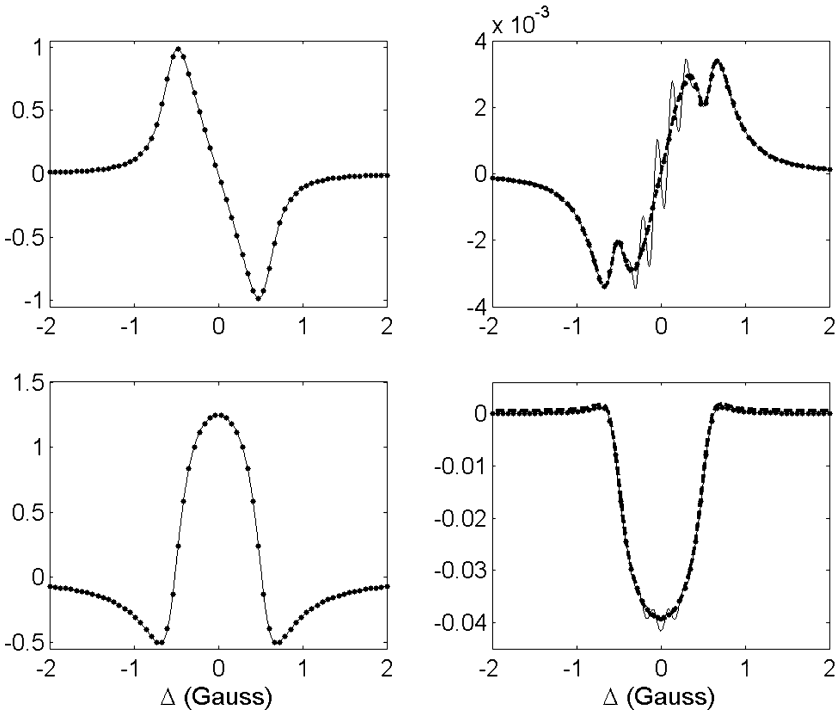

Fig. 2. First harmonic in-phase and quadrature line shapes: in-phase absorption/dispersion (left, top/bottom), quadrature absorption/dispersion (right, top/bottom). Relaxation rates are $R_2/\gamma = 140\,\mathrm{mG}$, $R_1/\gamma = 100\,\mathrm{mG}$, $\gamma h_1 \approx R_1, \gamma h_m = 8 \cdot R_2$, $\omega_m/2\pi = 10\,\mathrm{kHz}$. Solid thin lines (in all panels) are generated numerically from the direct diagonalization method with $N = 9$ (see text). "Dots" are generated from the continued fraction method $N = 10$ (see text). Dashed lines (right, top/bottom) are obtained from the in-phase absorption/dispersion signals (left, top/bottom) using Eqs. (12) and (13).

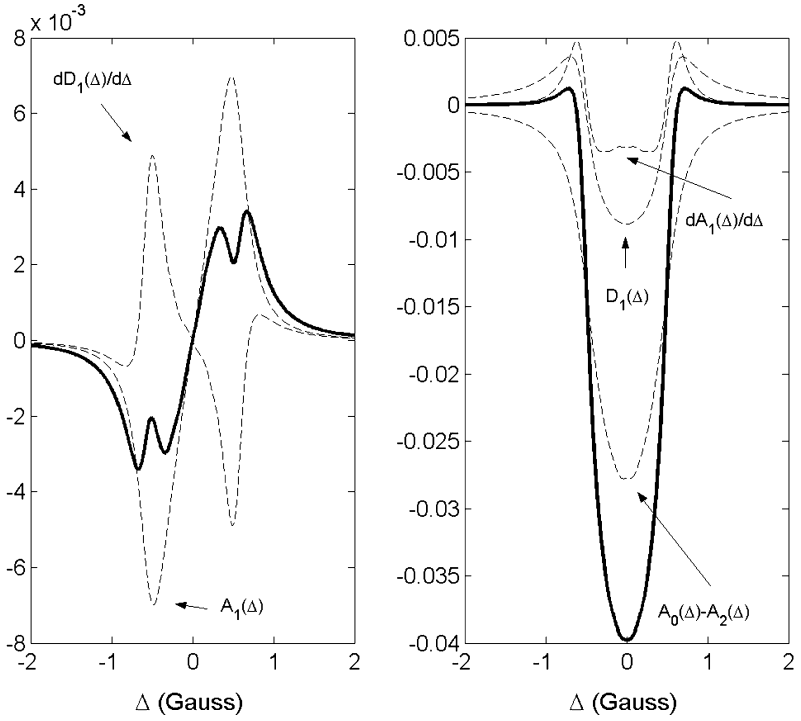

Fig. 3. First harmonic quadrature absorption (left) and dispersion (right) calculated using Eqs. (12) and (13) from in-phase signals that were generated numerically by direct diagonalization with $N = 9$ (see Fig. 2, right panels). The dark lines are the sum of the dashed lines. The text indicates the source of each contribution (dashed lines) to (12) and (13). The signals displayed are scaled by the coefficients from (12) and (13).

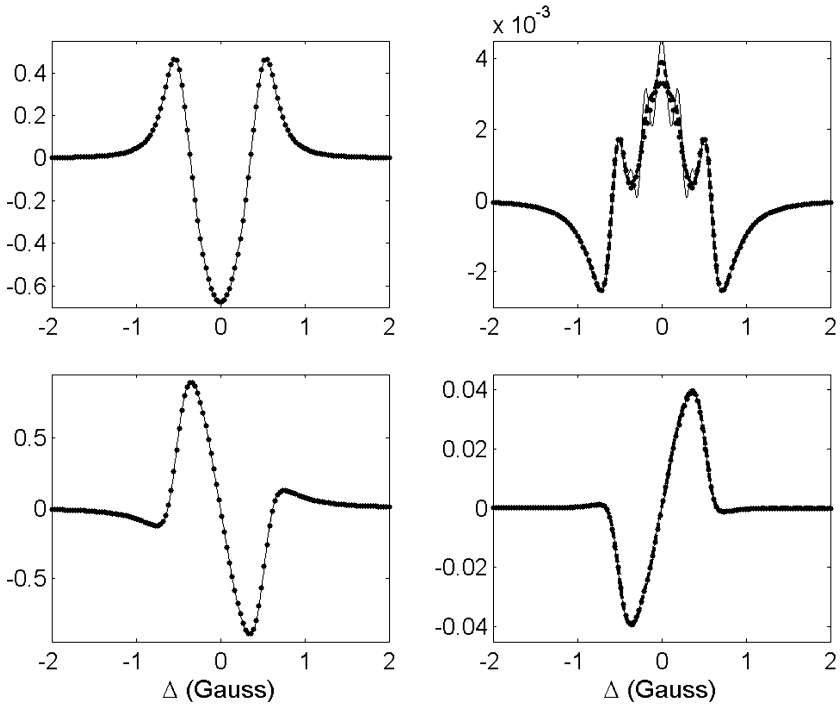

Fig. 4. Second harmonic in-phase and quadrature line shapes: in-phase absorption/dispersion (left, top/bottom), quadrature absorption/dispersion (right, top/bottom). Relaxation rates are the same as in Fig. 2, $\gamma h_1 \approx R_1$, $\gamma h_m = 8 \cdot R_2$, $\omega_m/2\pi = 10\,\text{kHz}$. Solid thin lines are generated numerically from the direct diagonalization method with $N = 9$ (see text). "Dots" are generated from the continued fraction method $N = 10$ (see text). Dashed lines (right, top/bottom) are obtained from the in-phase absorption/dispersion signals (left, top/bottom) using Eqs. (12) and (13).

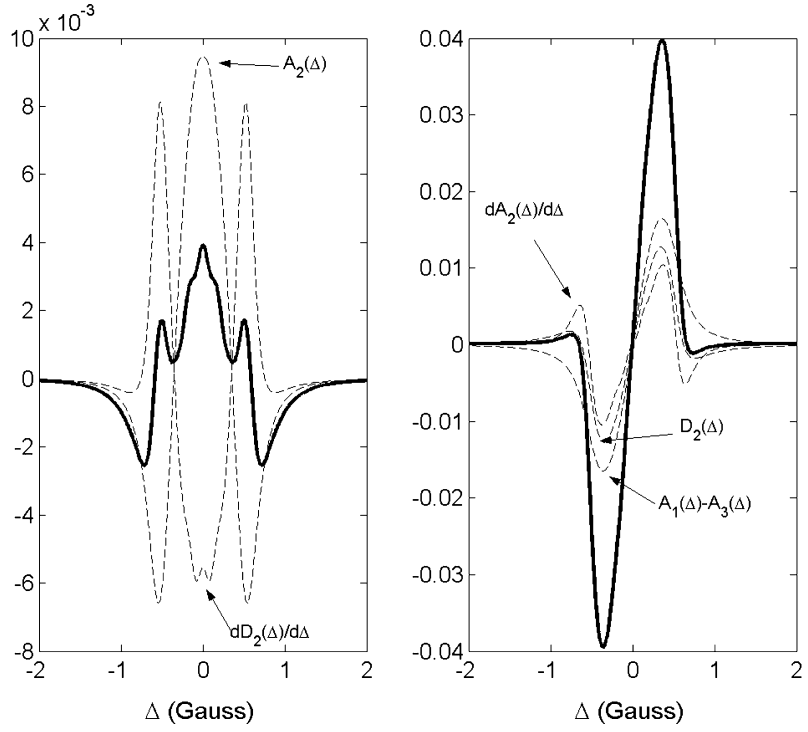

Fig. 5. Second harmonic quadrature absorption (left) and dispersion (right) calculated using Eqs. (12) and (13) from in-phase signals that were generated numerically by direct diagonalization with $N = 9$ (see Fig. 4, right panels). The dark lines are the sum of the dashed lines. The text indicates the source of each contribution (dashed lines) to (12) and (13). The signals displayed are scaled by the coefficients from (12) and (13).

numerically using the continued fraction approach. The dashed lines in the right panels are a test of Eqs. (12) and (13), and were constructed using only the in-phase signals in the left panels. The dashed lines in the right panels are linear combinations of the direct diagonalization-generated in-phase signals (shown in the left panels) using Eq. (12) in the case of absorption (top right) and using Eq. (13) in the case of dispersion (bottom right). The quadrature signals generated by the continued fraction method are also plotted (as dots) in the right panels, but are obscured by overlap with the dashed lines.

Fig. 3 shows the decomposition of the quadrature signals (from Fig. 2) into their components (absorption left and dispersion right) according to Eqs. (12) and (13). Because numerical derivatives of in-phase signals were necessary for Figs. 2 and 3, the signals were generated with a resolution of 4096 points over ±5 G to ensure accuracy. There are "extra" features in the quadrature signals generated from direct diagonalization, as seen in Fig. 2 (solid thin lines, right panels). These arise from finite truncation of the matrices. The truncation was at the 9th harmonic in Figs. 2 and 3. If the matrices had been truncated at higher harmonics these truncation errors would have been diminished. The 9th harmonic was deliberately chosen here so that the numerical result of the direct diagonalization procedure could be distinguished visually from the other methods, and to illustrate the effect of finite truncation.

Figs. 4 and 5 are the second harmonic analogues of Figs. 2 and 3. The numerically generated second harmonic quadrature absorption (Fig. 4, top right) exhibits the same type of deliberate truncation error as was observed in the first harmonic (Fig. 2, top right). The quadrature signals generated by the continued fraction method are plotted (as dots) in the right panels, but are obscured by overlap with the dashed lines. Fig. 5, shows the composition of the quadrature signals from Fig. 4 using expressions (12) and (13) for the second harmonic quadrature components.

4.2. Test of the filter formulation of modulation

Figs. 6–12 illustrate the action of the filters shown in Fig. 1 on numerically generated solutions to the Bloch equation that were obtained using the continued fraction method. The filters generate modulated line shapes by acting on the low modulation amplitude limit of either the first or second harmonic signals. Figs. 6 and 7 show the low modulation amplitude limit of the first and second harmonic in-phase and quadrature signals generated by the continued fraction method with the same parameters as used above in Figs. 2–5, except that the modulation amplitude is one-tenth the natural line width. As will be shown below, the spectra in Figs. 6 and 7, when properly filtered, will re-produce the over-modulated signals already given in Figs. 2–5.

Fig. 8 shows the application of the first harmonic filter (Eq. (6), f_{11} in Fig. 1) to each of the spectra in Fig. 6. The modulation width used in the filter was $\gamma h_m = 8 \cdot R_2$ so that the results could be directly compared with the numerically generated spectra having the same parameters as in Fig. 2. The dark lines are the simulations of the Bloch equation from the continued fraction method, just as in Fig. 2, but with greater resolution. The dashed lines are the application of the filter (6) to the spectra in Fig. 6 with no adjustment except a slight offset along the field axis for visualization. The filter (6) accurately reproduces the modulated first harmonic spectra using only the low modulation limit line shape as an input and no adjustable parameters. The second harmonic spectra in Fig. 7 are similarly filtered to produce modulated spectra using the filter (9) (f_{22} in Fig. 1). The action of filter (9) is depicted in Fig. 9 (dark dashed lines), and is the second harmonic analog of Fig. 8. The modulated second harmonic signals are alternatively generated from the low modulation limit of the *first* harmonic signals according to the filter (8) (f_{12} in Fig. 1). The result of applying filter (8) to the spectra in Fig. 6 is also shown in Fig. 9 (light dashed lines). Both sets of dashed lines are shifted along the field axis for visualization.

Excellent agreement is demonstrated in Figs. 8 and 9 between numerical solutions to the Bloch equation independently generated under high modulation ($\gamma h_m = 8 \cdot R_2$) and the result of applying filters (6), (8), and (9) to low modulation spectra ($\gamma h_m = 0.1 \cdot R_2$). The theoretical justification for all of these results rests upon a first order treatment of the modulation frequency ω_m, as detailed in the Appendix.

To demonstrate the break down of Eqs. (6), (8), and (9) and (10)–(13) away from the linear regime of modulation frequency, ω_m was increased by an order of magnitude from the value used in Figs. 2–9. As a first test, Fig. 10 shows Fig. 2 reproduced with the new modulation frequency $\omega_m/2\pi = 100$ kHz. The solid thick black lines are the numerical solutions to the Bloch equation using the continued fraction method, which properly include modulation to all orders. The thin solid lines are numerical simulations using the direct diagonalization method to first order in the modulation frequency (see Eq. (A.5) in the Appendix). The thick dashed lines (right panels) are Eqs. (12) and (13) applied to the in-phase continued fraction simulations. The thin solid lines are obscured in the right panels by overlap with the dashed lines. The numeric continued fraction method, because it is valid to all orders of modulation frequency, represents the correct line shape. The linearized approach of direct diagonalization (left panels, thin lines Fig. 10, Eq. (A.5)) resembles very closely the continued fraction simulation for the in-phase components (left panels, thick solid lines Fig. 10), but is slightly different at the maxima. The quadrature components calculated by the direct diagonalization show large deviations from

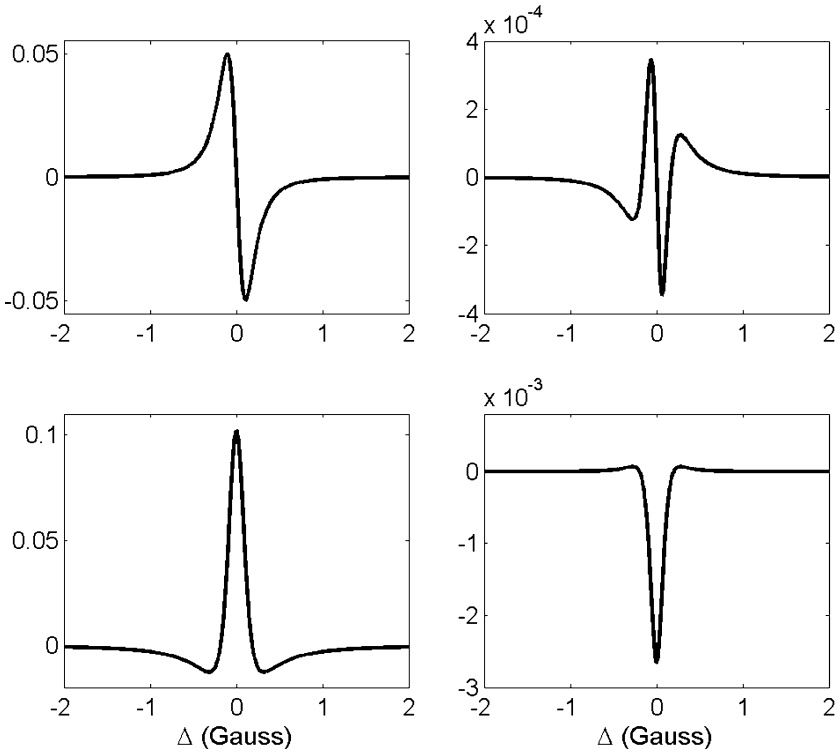

Fig. 6. First harmonic in-phase and quadrature line shapes: in-phase absorption/dispersion (left, top/bottom), quadrature absorption/dispersion (right, top/bottom). Relaxation rates are the same as in Fig. 2, $\gamma h_1 \approx R_1$, $\gamma h_m = 0.1 \cdot R_2$, $\omega_m/2\pi = 10\,\text{kHz}$. Spectra are generated from the continued fraction method $N = 10$ and a resolution of 4096 points over $\pm 5\,\text{G}$ (see text).

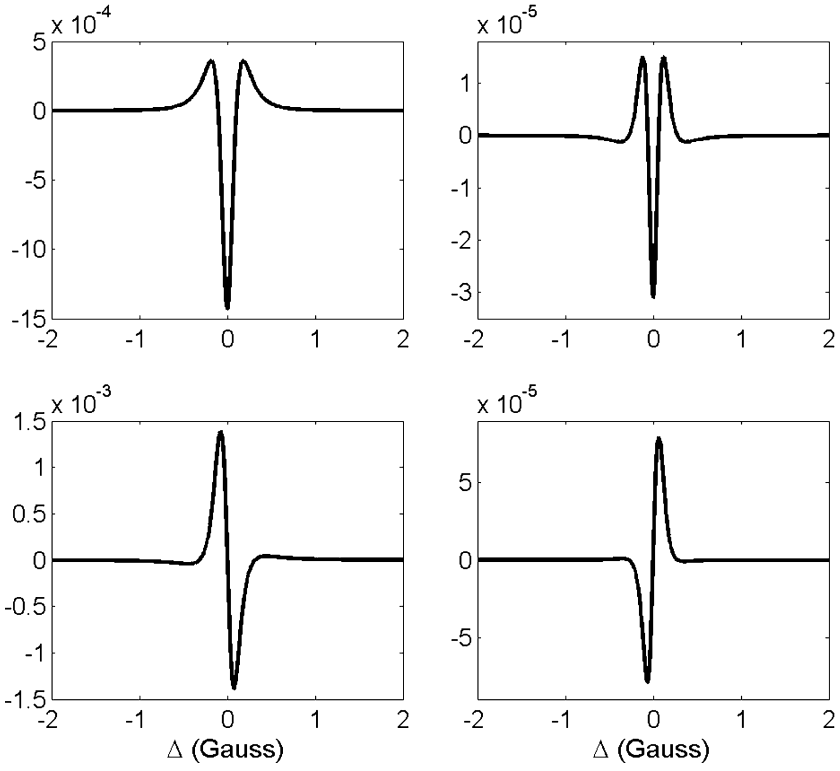

Fig. 7. Second harmonic in-phase and quadrature line shapes: in-phase absorption/dispersion (left, top/bottom), quadrature absorption/dispersion (right, top/bottom). Relaxation rates are the same as in Fig. 2, $\gamma h_1 \approx R_1$, $\gamma h_m = 0.1 \cdot R_2$, $\omega_m/2\pi = 10\,\text{kHz}$. Spectra are generated from the continued fraction method $N = 10$ and a resolution of 4096 points over $\pm 5\,\text{G}$ (see text).

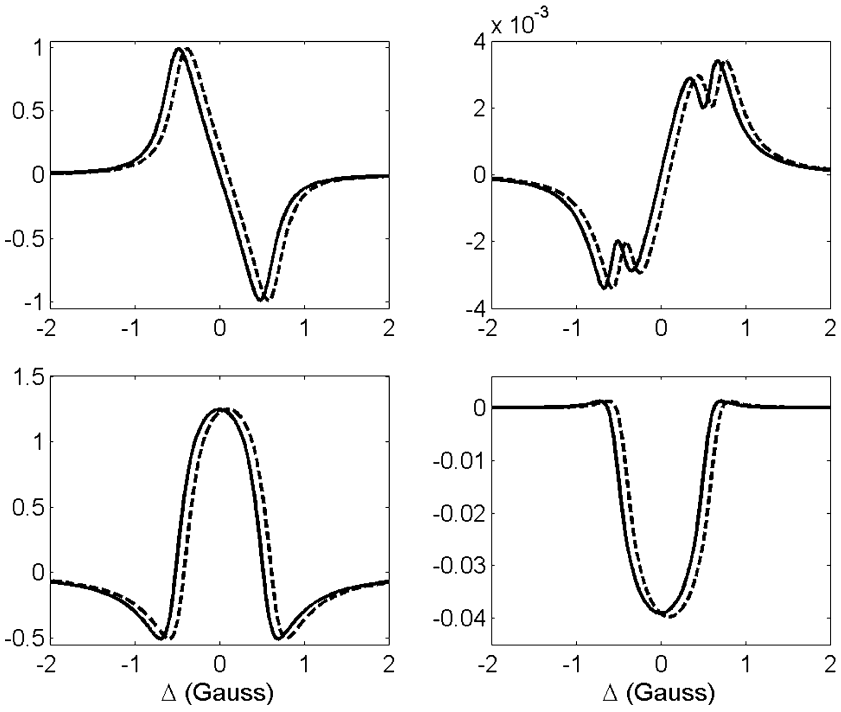

Fig. 8. First harmonic in-phase and quadrature line shapes: in-phase absorption/dispersion (left, top/bottom), quadrature absorption/dispersion (right, top/bottom). Solid lines are generated from the continued fraction method for $N = 10$ (see text) with parameters identical to Fig. 2. Dashed lines are the result of applying f_{11} (Eq. (7)) to each of the signals in Fig. 6. The modulation width in the filter was $\gamma h_m = 8 \cdot R_2$. The dashed lines have been translated slightly along the x-axis for visualization.

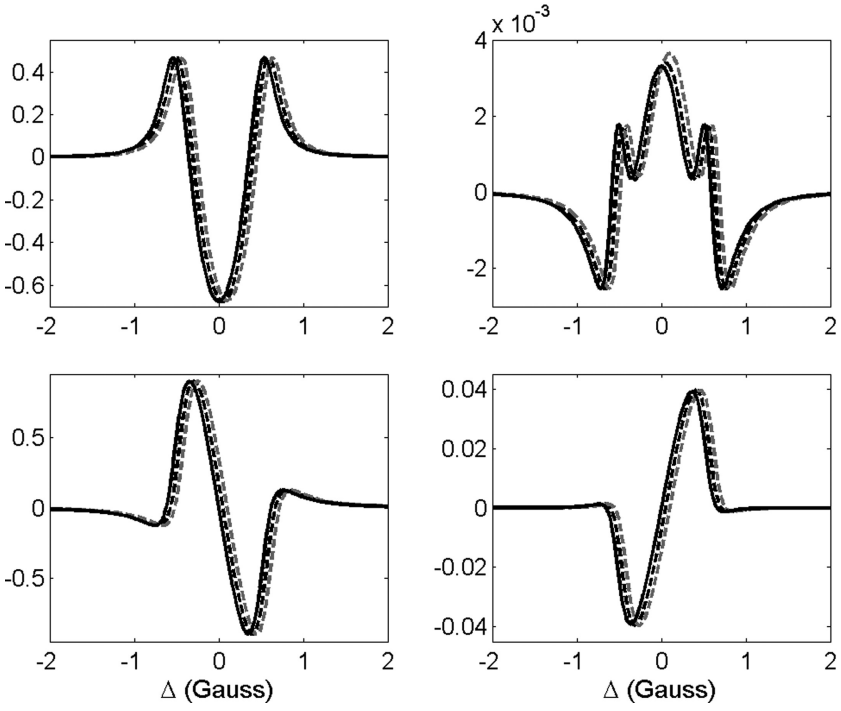

Fig. 9. Second harmonic in-phase and quadrature line shapes: in-phase absorption/dispersion (left, top/bottom), quadrature absorption/dispersion (right, top/bottom). Solid lines are generated from the continued fraction method for $N = 10$ (see text) with parameters identical to Fig. 4. The dark dashed lines are the result of applying f_{22} (Eq. (9)) to each of the signals in Fig. 7. The light dashed lines are the result of applying f_{12} (Eq. (8)) to each of the signals in Fig. 6. The modulation width in the each filter was $\gamma h_m = 8 \cdot R_2$. The dashed lines have been translated slightly along the x-axis for visualization.

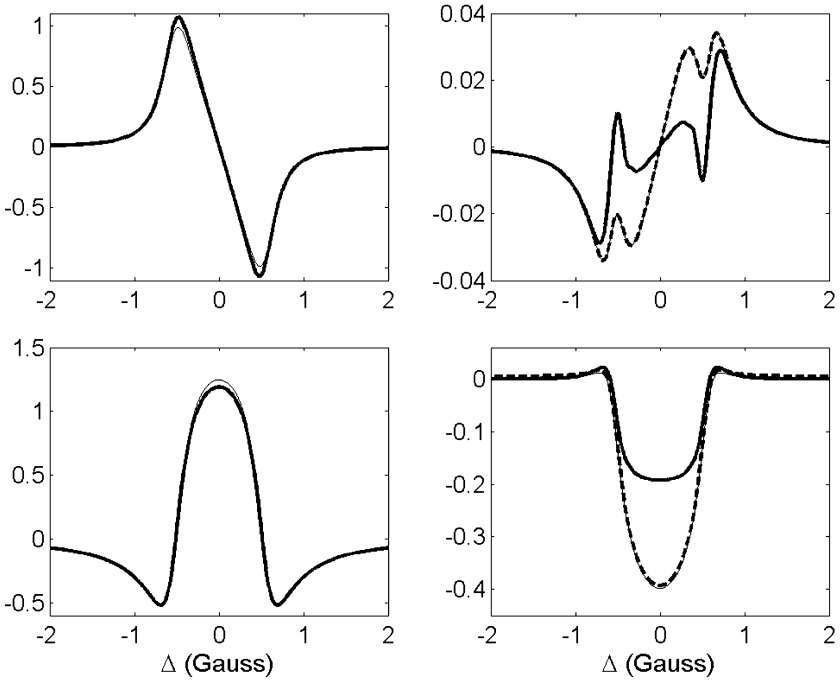

Fig. 10. First harmonic in-phase and quadrature line shapes: in-phase absorption/dispersion (left, top/bottom), quadrature absorption/dispersion (right, top/bottom). Relaxation rates are the same as in Fig. 2, $\gamma h_1 \approx R_1$, $\gamma h_m = 8 \cdot R_2$, $\omega_m/2\pi = 100$ kHz. Solid thin lines are generated numerically from the direct diagonalization method with $N = 9$ (see text), and are obscured in the right panels because of overlap with the dashed lines. Solid thick lines are generated from the continued fraction method for $N = 10$ (see text). Dashed lines (right, top/bottom) are obtained from the in-phase absorption/dispersion signals of the continued fraction method (left , top/bottom, thick lines) using equations (see text Eqs. (12) and (13)).

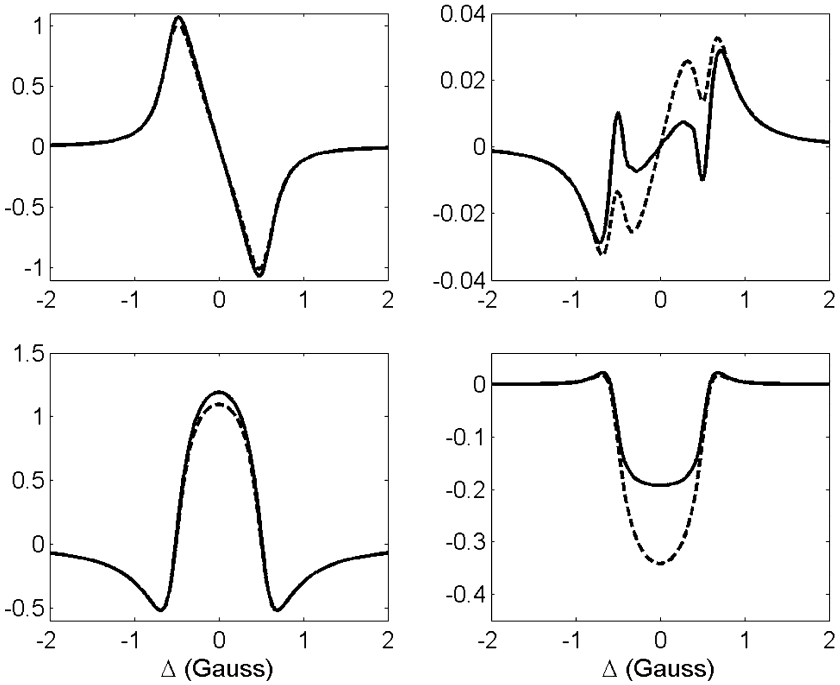

Fig. 11. First harmonic in-phase and quadrature line shapes: in-phase absorption/dispersion (left, top/bottom), quadrature absorption/dispersion (right, top/bottom). Relaxation rates are the same as in Fig. 2, $\gamma h_1 \approx R_1$, $\gamma h_m = 8 \cdot R_2$, $\omega_m/2\pi = 100$ kHz. Solid lines are generated from the continued fraction method for $N = 10$ and a resolution of 4096 points over ±5 G (see text). Dashed lines are generated from the filter (6) applied to low modulation amplitude spectra ($\gamma h_m = 0.1 \cdot R_2$) that were simulated with the continued fraction algorithm at $\omega_m/2\pi = 100$.

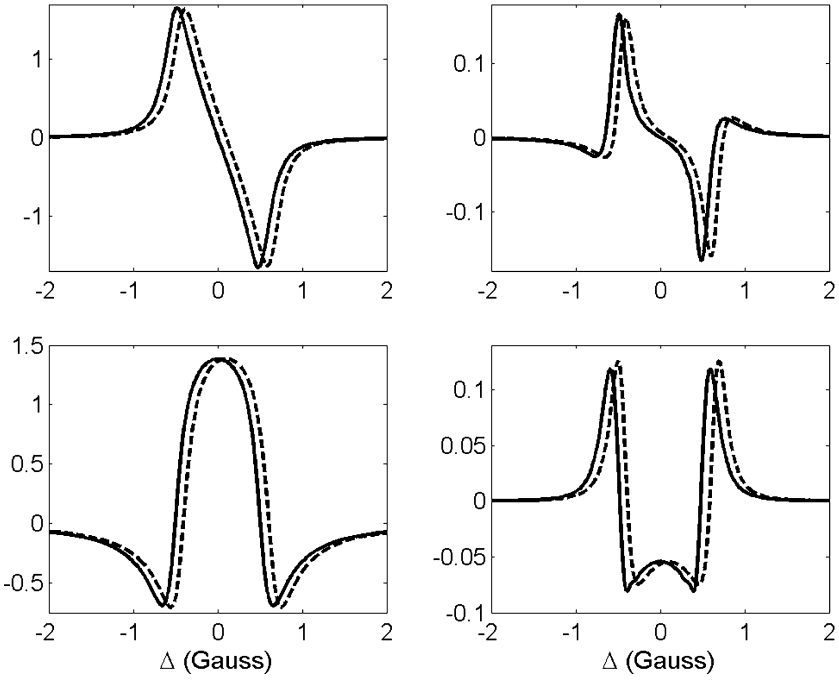

Fig. 12. First harmonic in-phase and quadrature line shapes: in-phase absorption/dispersion (left, top/bottom), quadrature absorption/dispersion (right, top/bottom). The parameters are identical to Fig. 11 except that $\gamma h_1 \approx R_1/10^2$. Solid lines are generated from the continued fraction method for $N = 10$ and a resolution of 4096 points over ±5 G (see text). Dashed lines are generated from low modulation amplitude spectra ($\gamma h_m = 0.1 \cdot R_2$) at $\omega_m/2\pi = 100$ and $\gamma h_1 \approx R_1/10^2$ using the filter (7).

the continued fraction line shapes, however. The representation of quadrature components as the superposition of in-phase signals (dashed lines) clearly breaks down. In fact, the quadrature signal calculated from a superposition of in-phase signals is in very good agreement with the linearized direct diagonalization calculation (thin lines, right panel), as would be suspected from the similarity of signals from the two simulation methods used in the left panels of Fig. 10.

To test the effect of modulation frequency on the filter method of Eq. (6), low modulation amplitude ($\gamma h_m = 0.1 \cdot R_2$) spectra were simulated with $\omega_m/2\pi = 100$ kHz using the continued fraction approach, in analogy to Fig. 6. The result of filtering these signals with Eq. (6) is shown in Fig. 11. The solid lines represent the same continued fraction calculation as in Fig. 10. The dashed lines are the filtered low modulation frequency signals using a filter modulation width of $\gamma h_m = 8 \cdot R_2$.

The filtered line shapes in Fig. 11 (dashed lines) retain the appearance of the spectra calculated under low modulation frequency in Figs. 2 and 8, and the numerical simulations linearized in ω_m using the direct diagonalization method in (thin lines in Fig. 10). The correct quadrature line shapes, with distortion due to non-linear modulation frequency effects (Fig. 11, solid lines), are quite different in the appearance from the filter predicitons. There are two possible sources that account for the poor agreement of the predicted quadrature signals in Figs. 10 and 11 with the exact calculations. Linearization of the Bloch equation with respect to modulation frequency involved two distinct approximations. First, only terms linear in the matrix **W** are retained (see definitions in Appendix). This is because the matrix **W** contains a factor of ω_m. **W** possesses an additional dependence on ω_m through the saturation term $S_n = (\gamma h_1)^2/((n\omega_m)^2 + R_1^2)$. The matrix **A** has a similar dependence on S_n. The values of γh_1 used in all of the figures above were partially saturating, i.e., $S_0 \approx 1$. Decreasing the microwave amplitude γh_1 diminishes the significance of S_n, and so diminishes the significance of the approximation $S_n \approx S_0$.

Fig. 12 is completely analogous to Fig. 11 except that γh_1 is diminished in Fig. 12 by two orders of magnitude from the value used in Fig. 11, so that $S_0 \approx 1/10^4$. The complete agreement found in Fig. 12 between the numerically generated spectra from the continued fraction method and the filtered low modulation amplitude spectra show that the approximation $S_n \approx S_0$ is responsible for the poor agreement in Fig. 11. This stresses the importance of competition between the value of microwave amplitude γh_1, R_1, and ω_m through the factor $S_n = (\gamma h_1)^2/((n\omega_m)^2 + R_1^2)$. If the microwave amplitude is appreciable enough to make S_n significant, the denominator $(n\omega_m)^2 + R_1^2$ must be dominated by R_1 for pseudo-modulation and the filters presented herein to rigorously hold.

In the Appendix, all quadratic terms $(n\omega_m)^2$ were neglected as part of the linear expansion in modulation frequency. At the same time, however, all harmonics were

included. The physicality of the linear expansion in ω_m is determined by the magnitude of the neglected higher order terms. The number of Fourier harmonics that contribute to the signal is influenced by the direct factor of ω_m in the definition of **W**, as well as the S_n dependence when the higher order terms in the modulation frequency are included. The method used in the Appendix to analytically solve the Bloch equations is not easily adapted to calculation of higher terms. The examples in this section, showing over-modulation with saturation, demonstrate, however, that the linear approximation is robust enough to encompass conditions that are often satisfied in typical EPR (modulation frequencies of 10 kHz with saturation, and 100 kHz without saturation). The examples in Section 5 show experimental tests of the filters.

5. Application of modulation filters to experimental CW spectra

Two systems were chosen to experimentally test the filters shown in Fig. 1. The first system is a double stranded 50-mer DNA fragment that is ^{15}N spin labeled. The DNA spectra shown here were acquired at room temperature. The preparation of the DNA is described elsewhere [20]. The dynamics of the DNA spin label are well characterized [20]. The second system studied is [^{15}N]maleimide spin labeled bovine serum albumin (BSA) at 2 °C in 60% glycerol/water and 0.1 mM. Spin labeled BSA has been well studied and an isotropic rotational correlation time of 1 μs has been assigned under these conditions [21].

5.1. Results

Figs. 13–15 show the in-phase first harmonic and second harmonic absorption spectra of the 50-mer DNA under low microwave amplitude (0.04 G). The experimental spectra are shown in light solid lines. The top spectra are obtained with modulation amplitude of 1 G and a modulation frequency of 15 kHz. The bottom spectra have 5 G modulation amplitude and 62 kHz modulation frequencies. The dark solid lines (bottom) are the result of applying f_{11} (Fig. 13), f_{12} (Fig. 14) or f_{22} (Fig. 15) to the top spectrum in each figure using the filter modulation width $h_m = 5$ G.

Figs. 16 and 17 are the in-phase first and second harmonic absorption obtained with higher microwave amplitude ($h_1 = 0.36$ G), and are the high microwave amplitude analogs of Figs. 13 and 14. Fig. 18 is the second harmonic quadrature signal and the filter prediction obtained from the first harmonic quadrature signal by f_{12} (see Fig. 1).

Figs. 19–21 show the in-phase first harmonic absorption and quadrature second harmonic absorption spectra of ^{15}N labeled BSA in 60% glycerol at 2 °C. Experimental spectra are shown with light lines, and were acquired with 0.34 G microwave amplitude and 50 kHz modulation frequency. The modulation amplitudes of the top spectra are 0.5 G, and the modulation amplitudes of the bottom spectra are 3.88 G. The dark lines (bottom) are obtained by applying f_{11} (Fig. 19), f_{12} (Fig. 20) or f_{22} (Fig. 21) to the top spectra.

The applications of the various filters to the low modulation spectrum illustrate that the filters reduce the noise in the spectrum (see in particular Figs. 15 and 21). Fig. 22 compares the use of filter f_{22} with a quadratic Savitzky–Golay filter [22].

5.2. Discussion of results

The application of the three modulation filters shown in Fig. 1 to the in-phase and quadrature first and second harmonic absorption signals of the 50-mer DNA are remarkable in several respects. The signals obtained by filtering the low modulation experimental spectra show excellent agreement with their experimentally over-modulated counterparts, which have a 62 kHz modulation frequency. The only input parameter to the filter function is the modulation width. The width was chosen to be the experimental modulation amplitude, which was pre-calibrated by over-modulating a single narrow resonance line [16]. The amplitude of the over-modulated signal is correctly predicted based solely on the low modulation input; there was no arbitrary scale adjustment of the filter outputs in the above figures. The input to the filter assumes that that the "low" modulation input is acquired with sufficiently small modulation amplitude that the spectrum approximates the derivative of the un-modulated signal. In practice, this means that the shape of the signal should not change if the modulation amplitude is lowered. The filters cannot be applied to an already over-modulated line shape, because they are non-additive. For example, a filter with a 5 G width could not be applied to the *bottom* spectrum in Fig. 13 (experimental modulation amplitude of 5 G) to produce the 10 G over-modulated spectrum. A modulation amplitude of 1 G was used as the low modulation condition for the spin labeled DNA, because no distortion was observed at lower values of the modulation amplitude. The first harmonic low modulation input to the filter must be scaled by the experimental modulation amplitude that was used to acquire the low modulation input, and the low modulation amplitude second harmonic input must be scaled by the square of the experimental modulation amplitude. The results from the DNA sample demonstrate that the conventional EPR signal contains all of the information present in the over-modulated higher modulation frequency signal. The low modulation quadrature signals must be rescaled by the ratio of experimental modulation frequencies when used as an input

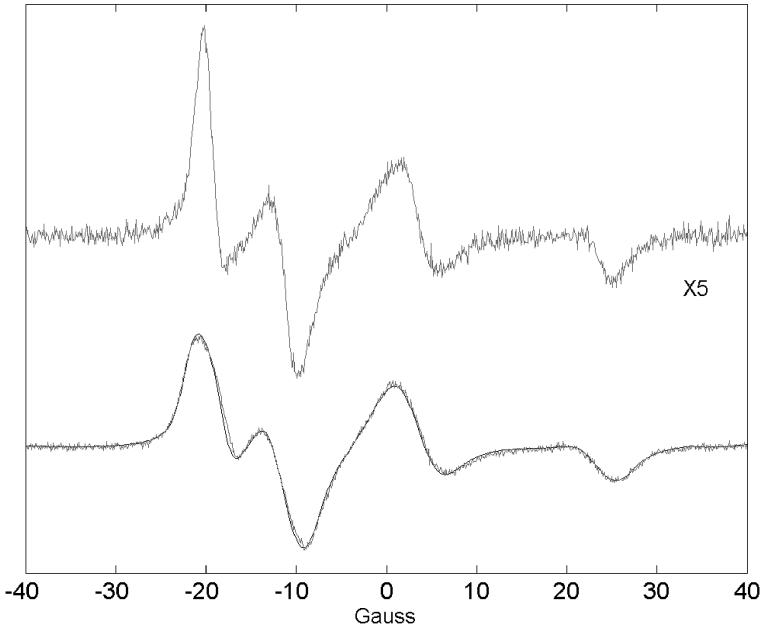

Fig. 13. In-phase first harmonic absorption spectrum of ^{15}N spin labeled DNA, room temperature. Light lines are experimental spectra with $h_1 = 0.04\,G$. (Top) $h_m = 1\,G$ and $\omega_m/2\pi = 15\,kHz$. (Bottom) $h_m = 5\,G$ and $\omega_m/2\pi = 62\,kHz$. The dark solid line (bottom) is the result of applying f_{11} (see Eq. (6) and Fig. 1) to the top spectrum with filter width $h_m = 5\,G$.

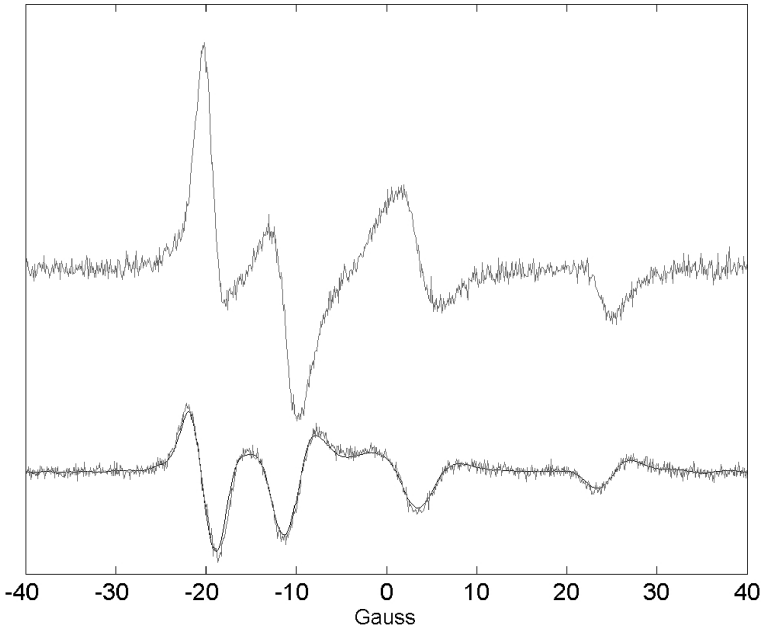

Fig. 14. In-phase first harmonic and second harmonic absorption spectrum of ^{15}N spin labeled DNA, room temperature. Light lines are experimental spectra with $h_1 = 0.04\,G$. (Top) First harmonic absorption, $h_m = 1\,G$ and $\omega_m/2\pi = 15\,kHz$. (Bottom) Second harmonic absorption, $h_m = 5\,G$ and $\omega_m/2\pi = 62\,kHz$. The dark solid line (bottom) is the result of applying f_{12} (see Eq. (8) and Fig. 1) to the first harmonic spectrum (top) with filter width $h_m = 5\,G$.

to the modulation filters (see Eqs. (12) and (13)) if the filtered signal is to be compared with the higher frequency signal on the same absolute scale.

The examples shown illustrate the noise-filtering capabilities of the modulation filters. We suggest that the filters exhibited here could be used in place of common noise filters such as the Savitzky–Golay filter (see Fig. 22) or the 1–2–1 filter [22]. In this way spectra could be filtered for noise reduction, and any possible distortion would be manifest as over-modulation. Fig. 14 shows that the noise is reduced and the over-modulated signal is reproduced. More importantly, Fig. 14 shows that

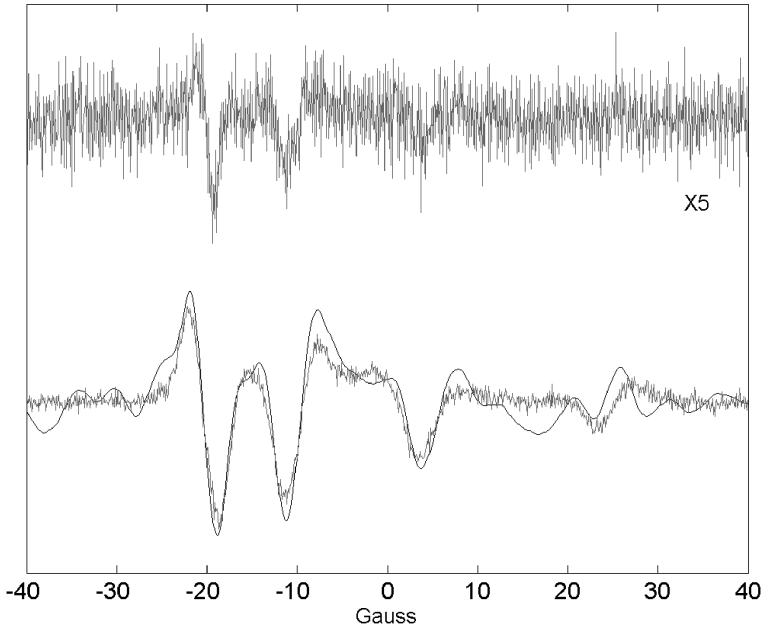

Fig. 15. In-phase second harmonic absorption spectrum of ^{15}N spin labeled DNA, room temperature. Light lines are experimental spectra with $h_1 = 0.04$ G. (Top) $h_m = 1$ G and $\omega_m/2\pi = 15$ kHz. (Bottom) $h_m = 5$ G and $\omega_m/2\pi = 62$ kHz. The dark solid line (bottom) is the result of applying f_{22} (see Eq. (9) and Fig. 1) to the top spectrum with filter width $h_m = 5$ G.

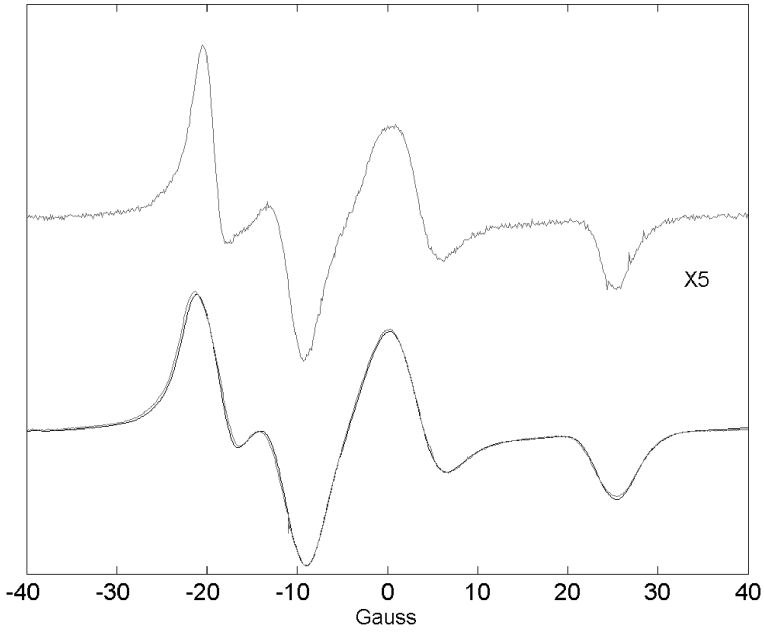

Fig. 16. In-phase first harmonic absorption spectrum of ^{15}N spin labeled DNA, room temperature. Light lines are experimental spectra with $h_1 = 0.36$ G. (Top) $h_m = 1$ G and $\omega_m/2\pi = 15$ kHz. (Bottom) $h_m = 5$ G and $\omega_m/2\pi = 62$ kHz. The dark solid line (bottom) is the result of applying f_{11} (Eq. (6) see Fig. 1) to the top spectrum with filter width $h_m = 5$ G.

the modulation filter f_{12} (see Fig. 1) is able to reproduce the second harmonic signal with only the information contained in the under-modulated first harmonic signal as an input. Not only is over-modulation taken into account properly, but also the over-modulated second harmonic signal is shown to contain no more information than is in the under-modulated first harmonic signal. The example using BSA (Fig. 20), however, shows how the filter, f_{12}, relating the first and second harmonic signals breaks down when STEPR conditions apply. Finally, the DNA spectra used here are a rigorous test of the filter methods. The DNA spectra cannot be simulated by the simple Bloch equation, because the spectra are not in the fast-motion regime [20]. A proper simulation

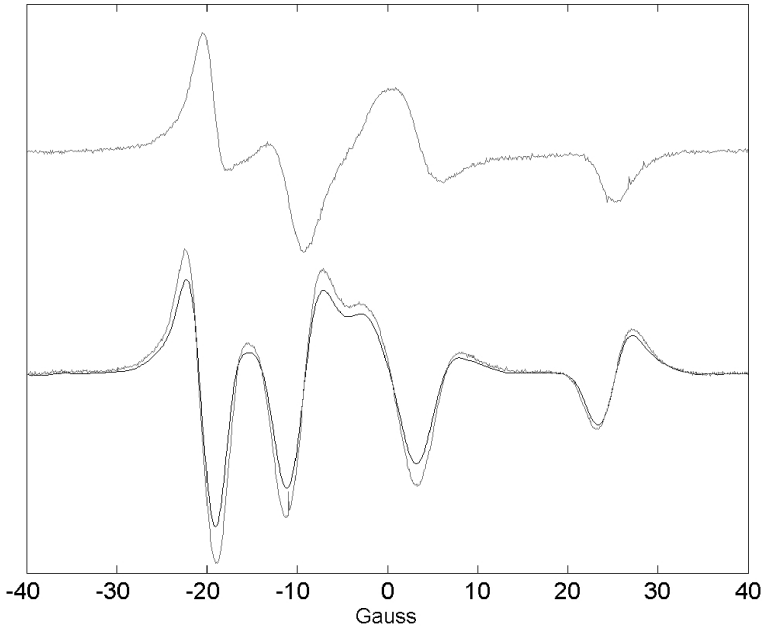

Fig. 17. In-phase first harmonic and in-phase second harmonic absorption spectrum of ^{15}N spin labeled DNA, room temperature. Light lines are experimental spectra with $h_1 = 0.36$ G. (Top) First harmonic absorption, $h_m = 1$ G and $\omega_m/2\pi = 15$ kHz. (Bottom) second harmonic absorption, $h_m = 5$ G and $\omega_m/2\pi = 62$ kHz. The dark solid line (bottom) is the result of applying f_{12} (see Eq. (8) and Fig. 1) to the first harmonic spectrum (top) with filter width $h_m = 5$ G.

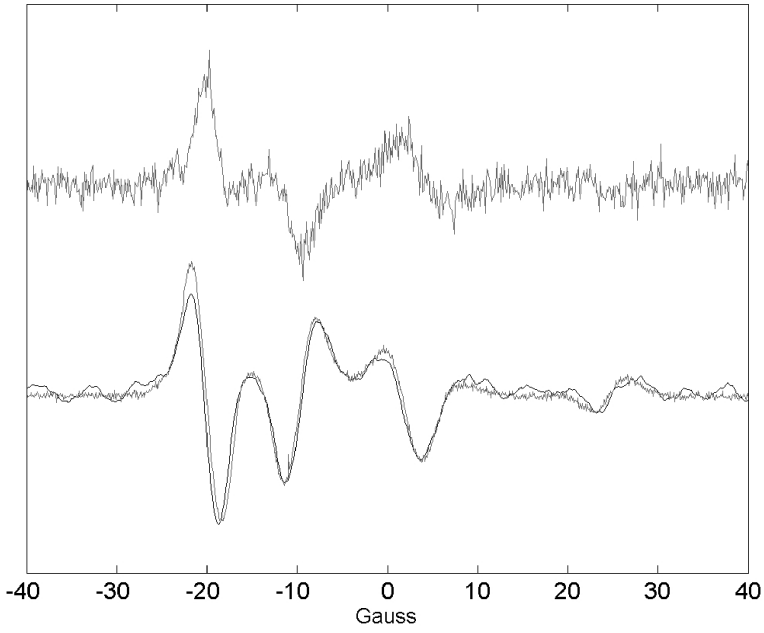

Fig. 18. Quadrature first harmonic and quadrature second harmonic absorption spectrum of ^{15}N spin labeled DNA, room temperature. Light lines are experimental spectra with $h_1 = 0.36$ G. (Top) First harmonic absorption, $h_m = 1$ G, and $\omega_m/2\pi = 15$ kHz. (Bottom) Second harmonic absorption, $h_m = 5$ G and $\omega_m/2\pi = 62$ kHz. The dark solid line (bottom) is the result of applying f_{12} (see Eq. (8) and Fig. 1) to the first harmonic spectrum (top) with filter width $h_m = 5$ G.

of the DNA spectrum would have to account for the influence of global dynamic modes (tumbling of the DNA about its center of mass) and the local motion (bending and flexing of the DNA). The fact that the spectra represent the influence of multiple dynamic processes, yet are still amenable to simple filtration to account for over-modulation is remarkable, and testifies to the fact that the effect of modulation on the DNA spectra is not dynamic but is simply an averaging of the low modulation spectrum. The fact that the in-phase absorption signals are filterable at low and high microwave amplitude does not completely test the filter methods (see Section 4). The

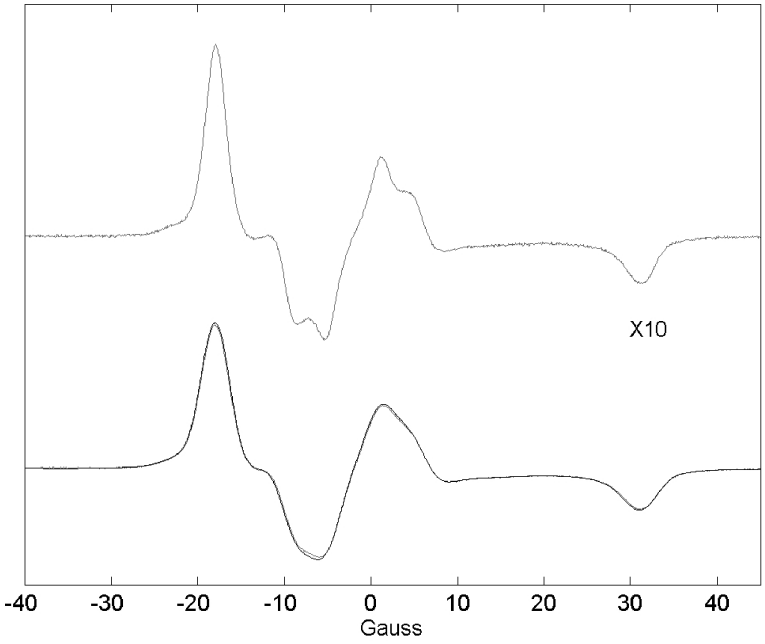

Fig. 19. In-phase first harmonic absorption spectrum of ^{15}N BSA in 60% glycerol/water at 2 °C. Light lines are experimental spectra with $h_1 = 0.34$ G. (Top) $h_m = 0.5$ G and $\omega_m/2\pi = 50$ kHz. (Bottom) $h_m = 3.88$ G and $\omega_m/2\pi = 50$ kHz . The dark solid line (bottom) is the result of applying f_{11} (Eq. (6) see Fig. 1) to the top spectrum with filter width $h_m = 3.88$ G.

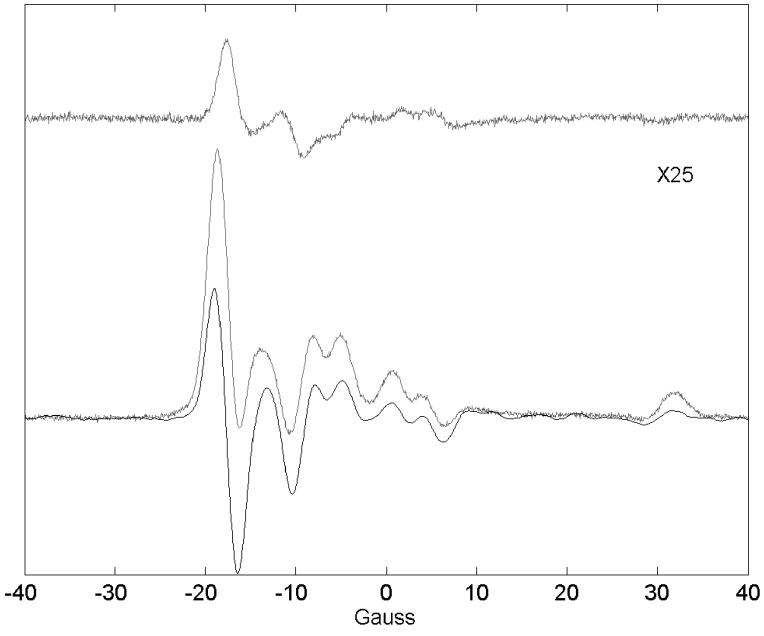

Fig. 20. Quadrature first harmonic absorption and quadrature second harmonic absorption spectra of ^{15}N \BSA in 60% glycerol/water at 2 °C. Light lines are experimental spectra with $h_1 = 0.34$ G. (Top) First harmonic absorption, $h_m = 0.5$ G and $\omega_m/2\pi = 50$ kHz. (Bottom) Second harmonic absorption, $h_m = 3.88$ G and $\omega_m/2\pi = 50$ kHz . The dark solid line (bottom) is the result of applying f_{12} (see Eq. (8) and Fig. 1) to the first harmonic spectrum (top) with filter width $h_m = 3.88$ G.

quadrature signals are more sensitive to the influence of dynamics and modulation frequency. The f_{12} filter was tested on the DNA sample using the first harmonic under-modulated quadrature signal (Fig. 18). The under-modulated second harmonic quadrature signal did not posses sufficient signal-to-noise to give meaningful predictions using f_{22} for the DNA sample. The f_{22} filter was tested, however, on the second harmonic quadrature signal of spin labeled BSA, where a sufficient under-modulated second harmonic signal was obtained (Fig. 21).

The spin labeled BSA example gives an important test of the filter methods. BSA is a protypical example of a

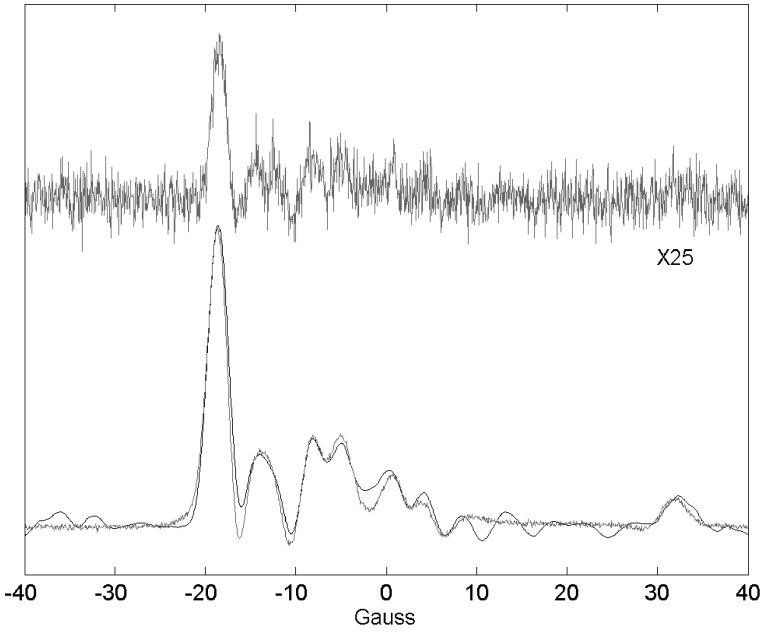

Fig. 21. Quadrature second harmonic absorption spectrum of ^{15}N BSA in 60% glycerol/water at 2 °C. Light lines are experimental spectra with $h_1 = 0.34$ G. (Top) $h_m = 0.5$ G and $\omega_m/2\pi = 50$ kHz. (Bottom) $h_m = 3.88$ G and $\omega_m/2\pi = 50$ kHz. The dark solid line (bottom) is the result of applying f_{22} (see Eq. (9) and Fig. 1) to the top spectrum with filter width $h_m = 3.88$ G.

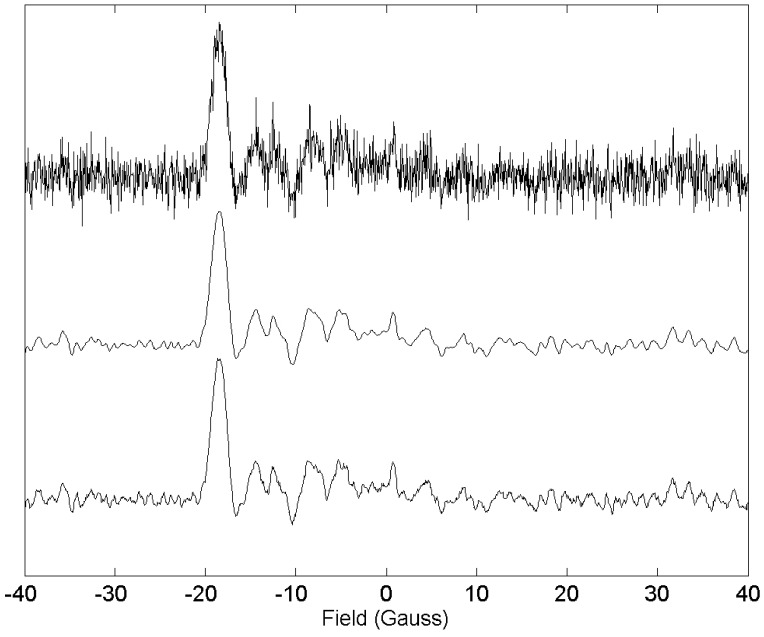

Fig. 22. Quadrature second harmonic absorption spectrum of ^{15}N BSA in 60% glycerol/water at 2 °C. (Top) Experimental spectrum with $h_1 = 0.34$ G, $h_m = 0.5$ G, and $\omega_m/2\pi = 50$ kHz. (Middle) Application of f_{22} (see Eq. (9) and Fig. 1) to the top spectrum with filter width $h_m = 1$ G. (Bottom) Application to the top spectrum of a quadratic Savitzky–Golay filter with a width of 1 G.

spin labeled biological molecule that has been studied by STEPR [23]. A non-trivial influence of modulation frequency should therefore be observable in the spin labeled BSA STEPR spectrum. The agreement found in Fig. 19, where the f_{11} is applied to the first harmonic in-phase spectrum, is not surprising given the success of the filter methods on the DNA spectra; but provides another demonstration that the filter is applicable with a modulation frequency as high as 50 kHz. Fig. 20 shows that the filter prediction of the second harmonic quadrature signal, using the first harmonic quadrature spectrum as an input, does not agree with the experimentally acquired second

harmonic spectrum. The filter prediction resembles the low modulation frequency second harmonic quadrature spectrum (not shown). The latter result is similar to the conclusion drawn from Fig. 11 in Section 4. Fig. 20 illustrates that the quadrature second harmonic (STEPR) spectrum contains information that is not reproducible from the first harmonic spectrum. Fig. 21 shows the application of f_{22} to the experimental under-modulated quadrature second harmonic spectrum of BSA (top). The filtered prediction is in excellent agreement with the experimental over-modulated second harmonic spectrum (bottom), especially considering the noise of the input spectrum. Figs. 20 and 21 show that while the f_{12} filter (applied to the first harmonic to obtain the second harmonic) may fail, the f_{22} filter from under-modulated second harmonic to over-modulated second harmonic gives a reasonable prediction of the effect of modulation. STEPR simulations that include a full treatment of molecular motion are often restricted to the low modulation amplitude limit because of the computational cost of including modulation. The empirical success of the filter f_{22} is promising. Theoretical STEPR quadrature signals can be filtered to account for the effect of over-modulation with minimal computational cost once the low modulation amplitude spectrum is simulated using conventional STEPR codes. This procedure has the potential to increase the efficiency of global optimization routines such as gradient searches, wherein many successive executions of the simulation routine are required. Once a best fit is found with the filter technique, a more accurate simulation that includes modulation directly [6,7] can be used to check the quality of the fit and further optimize the simulation.

6. Conclusions

Pseudo-modulation was reviewed in its original form. It was shown that pseudo-modulation is equivalent to a filter acting upon the low modulation amplitude limit spectrum. Pseudo-modulation was justified from the Bloch equation by analytic direct diagonalization of the infinite matrix form of the Bloch equation. The latter method allowed for the dispersion signal to be incorporated into the formalism of pseudo-modulation. The quadrature components were expressed, in the linear limit of modulation frequency, as simple linear functions of the in-phase absorption and dispersion components and their derivatives. The expression of the quadrature spectrum in terms of the in-phase components allowed the filter form of pseudo-modulation to be carried over to the quadrature components. Thus, the filter relations derived from pseudo-modulation were shown to cover the complete effect of modulation amplitude for all possible signals in the linear limit of modulation frequency. The possible applications and attendant complications of using the filter methods outside of the linear modulation frequency domain were illustrated numerically. The use of the filter methods for quadrature signals of STEPR spectra was discussed and demonstrated by application to both numerically and experimentally generated spectra. We found that the effect of over-modulation on in-phase signals was robustly captured by the filter functions, even for modulation frequencies as high as 50 kHz. The accuracy of filtered quadrature signals was observed to be more sensitive to deviation from the linear modulation frequency regime, especially at higher microwave powers, as anticipated from dependence of the microwave saturation contribution on the harmonic of modulation. The experimental tests of the filters suggest that over-modulation can be accounted for by applying the filters that act on the same harmonic as the target spectrum.

Acknowledgment

This work was supported in part by NIH GM65944, NIH R37 HL34737, the AFOSR and NIEHS.

Appendix A

The Bloch equation can be written in matrix form, with the additional modulating field included [9]. The Bloch equation is simplified by transforming to an external coordinate frame that precesses with the microwave frequency ω about the $\hat{z}$ axis.

$$\frac{\mathrm{d}}{\mathrm{d}t}\begin{pmatrix}\tilde{M}_x\\ \tilde{M}_y\\ \tilde{M}_z - M_0\end{pmatrix} = \begin{pmatrix}-R_2 & \Delta + \frac{\gamma h_{\mathrm{m}}}{2}\cdot\cos(\omega_{\mathrm{m}}\cdot t) & 0\\ -\Delta - \frac{\gamma h_{\mathrm{m}}}{2}\cdot\cos(\omega_{\mathrm{m}}\cdot t) & -R_2 & \gamma h_1\\ 0 & -\gamma h_1 & -R_1\end{pmatrix} \cdot \begin{pmatrix}\tilde{M}_x\\ \tilde{M}_y\\ \tilde{M}_z - M_0\end{pmatrix} + \begin{pmatrix}0\\ \gamma h_1 \cdot M_0\\ 0\end{pmatrix}. \tag{A.1}$$

The components of the magnetization are expanded in a Fourier series consisting of the harmonics of ω_{m}.

$$\begin{pmatrix}\tilde{M}_x(t)\\ \tilde{M}_y(t)\\ \tilde{M}_z(t) - M_0\end{pmatrix} = \sum_{r=0}^{\infty}\cos(n\cdot\omega_{\mathrm{m}}\cdot t)\cdot\begin{pmatrix}\mathrm{Disp}_n\\ \mathrm{Abs}_n\\ \mathrm{Long}_n\end{pmatrix} + \sin(n\cdot\omega_{\mathrm{m}}\cdot t)\cdot\begin{pmatrix}\mathrm{Disp}'_n\\ \mathrm{Abs}'_n\\ \mathrm{Long}'_n\end{pmatrix}.$$

The Fourier coefficients are labeled Disp_n for the nth cosine (in-phase) harmonic of the dispersion signal and Disp'_n for the nth sine (quadrature) harmonic of the dispersion signal. Likewise, Abs_n stands for the harmonics of absorption, and Long_n for the harmonics of the longitudinal magnetization. Substitution of the Fourier expansion into the Bloch equation and projection of the sine and cosine components gives an infinite set of coupled linear equations for the Fourier coefficients. It is convenient to generalize the index n to negative values. This just reproduces the in-phase coefficients ($\mathrm{Abs}_n = \mathrm{Abs}_{-n}$), and gives the negative of the quadrature coefficients ($\mathrm{Abs}'_n = -\mathrm{Abs}'_n$). The resulting equation for the in-phase and quadrature Fourier coefficients of absorption and dispersion is [9]:

$$(\mathbf{A}+\mathbf{W}+\mathbf{H})\cdot\chi = \mathbf{Z}_0, \tag{A.2}$$

where

$$\chi = \begin{pmatrix} \vdots \\ \chi_{-1} \\ \chi_0 \\ \chi_1 \\ \vdots \end{pmatrix}, \quad \chi_n = \begin{pmatrix} \mathrm{Abs}_n \\ \mathrm{Disp}_n \\ \mathrm{Disp}'_n \\ -\mathrm{Abs}'_n \end{pmatrix}, \quad \mathbf{Z}_0 = \begin{pmatrix} \vdots \\ 0 \\ \gamma h_1 \cdot M_0 \cdot \delta_{n,0} \\ 0 \\ 0 \\ \vdots \end{pmatrix}$$

$$\mathbf{A} = \begin{pmatrix} \ddots & 0 & 0 & 0 & 0 \\ 0 & \mathbf{A}_{-1} & 0 & 0 & 0 \\ 0 & 0 & \mathbf{A}_0 & 0 & 0 \\ 0 & 0 & 0 & \mathbf{A}_1 & 0 \\ 0 & 0 & 0 & 0 & \ddots \end{pmatrix},$$

$$\mathbf{A}_n = \begin{pmatrix} \Delta & -R_2 & 0 & 0 \\ R_2 + R_1 \cdot S_n & \Delta & 0 & 0 \\ 0 & 0 & \Delta & -(R_2 + R_1 \cdot S_n) \\ 0 & 0 & R_2 & \Delta \end{pmatrix}$$

with $S_n = (\gamma h_1)^2/((n\omega_\mathrm{m})^2 + (R_1)^2)$

$$\mathbf{W} = \begin{pmatrix} \ddots & 0 & 0 & 0 & 0 \\ 0 & \mathbf{W}_{-1} & 0 & 0 & 0 \\ 0 & 0 & \mathbf{W}_0 & 0 & 0 \\ 0 & 0 & 0 & \mathbf{W}_1 & 0 \\ 0 & 0 & 0 & 0 & \ddots \end{pmatrix},$$

$$\mathbf{W}_n = \begin{pmatrix} 0 & 0 & n\omega_\mathrm{m} & 0 \\ 0 & 0 & 0 & n\omega_\mathrm{m}(1-S_n) \\ n\omega_\mathrm{m}(1-S_n) & 0 & 0 & 0 \\ 0 & n\omega_\mathrm{m} & 0 & 0 \end{pmatrix},$$

$$\mathbf{H} = \begin{pmatrix} \ddots & \mathbf{H}_\mathrm{m} & 0 & 0 \\ \mathbf{H}_\mathrm{m} & 0 & \mathbf{H}_\mathrm{m} & 0 \\ 0 & \mathbf{H}_\mathrm{m} & 0 & \mathbf{H}_\mathrm{m} \\ 0 & 0 & \mathbf{H}_\mathrm{m} & \ddots \end{pmatrix}, \quad \mathbf{H}_\mathrm{m} = \frac{\gamma h_\mathrm{m}}{4} \cdot \begin{pmatrix} 1 & 0 & 0 & 0 \\ 0 & 1 & 0 & 0 \\ 0 & 0 & 1 & 0 \\ 0 & 0 & 0 & 1 \end{pmatrix}.$$

The infinite set of equations described by (A.2) can be converted to a matrix continued fraction consisting of 4×4 matrices. The matrix continued fraction is solved numerically by iteration assuming the continued fraction convergents become stable for large enough value of n [9].

The matrix $\mathbf{A}+\mathbf{W}+\mathbf{H}$ may be re-written using the nth convergent.

$$\mathbf{A}+\mathbf{W}+\mathbf{H} = \begin{pmatrix} \ddots & \mathbf{H}_\mathrm{m} & 0 & 0 & 0 \\ \mathbf{H}_\mathrm{m} & \mathbf{A}_0+\mathbf{W}_0 & \mathbf{H}_\mathrm{m} & 0 & 0 \\ 0 & \mathbf{H}_\mathrm{m} & \mathbf{A}_1+\mathbf{W}_1 & \ddots & 0 \\ 0 & 0 & \ddots & \ddots & \mathbf{H}_\mathrm{m} \\ 0 & 0 & 0 & \mathbf{H}_\mathrm{m} & \mathbf{C}_n \end{pmatrix}.$$

The $\mathbf{C}_{n-1}$ convergent is written in terms of $\mathbf{C}_n$ by Gaussian elimination.

$$\mathbf{C}_{n-1} = (\mathbf{A}_{n-1}+\mathbf{W}_{n-1}) - \mathbf{H}_\mathrm{m}^2 \cdot (\mathbf{C}_n)^{-1}. \tag{A.3}$$

This recurrence terminates at the $n = 0$ index because the elements of χ for negative index are not independent but $\mathrm{Abs}_n = \mathrm{Abs}_{-n}$, $\mathrm{Abs}'_n = -\mathrm{Abs}'_{-n}$, etc.The recurrence (A.3) is the matrix continued fraction algorithm that allows for iterative numerical solution. To begin the recurrence, it is assumed that for some large N the value of $\mathbf{C}_N$ is stable, i.e., $\mathbf{C}_N = \mathbf{C}_{N+1} = \cdots$ Eq. (A.3) then becomes a closed relation for $\mathbf{C}_N$ and gives:

$$\mathbf{C}_N = \frac{\mathbf{A}_N+\mathbf{W}_N}{2} + \sqrt{\left(\frac{\mathbf{A}_N+\mathbf{W}_N}{2}\right)^2 - \mathbf{H}_\mathrm{m}^2},$$

where the square root operation on matrices is interpreted in the eigenvalue sense. This is the continued fraction iteration.

In the direct diagonalization approach Eq. (A.2) is solved directly by truncating the infinite dimensional matrices $\mathbf{A}$, $\mathbf{W}$, and $\mathbf{H}$. Then, Eq. (A.2) is solved by standard diagonalization to give:

$$\chi = (\mathbf{A}+\mathbf{W}+\mathbf{H})^{-1}\cdot\mathbf{Z}_0. \tag{A.4}$$

We desire a solution to first order in ω_m. To first order in $\mathbf{W}$, the solution is given by:

$$\chi = ((\mathbf{A}+\mathbf{H})^{-1} - (\mathbf{A}+\mathbf{H})^{-1}\cdot\mathbf{W}\cdot(\mathbf{A}+\mathbf{H})^{-1})\cdot Z_0 \tag{A.5}$$

at the same time $\mathbf{A}$ simplifies because $S_n = S_0$ to first order in ω_m, and $\mathbf{A}$ is made of 4×4 blocks of $\mathbf{A}_0$.

The structure of the matrix $(\mathbf{A}+\mathbf{H})^{-1}$ is essential for an understanding of how the solution relates to the

pseudo-modulation formula.The sub-matrix $\mathbf{A}_0$ is diagonalized by $U_{\mathbf{A}_0}$:

$$U_{\mathbf{A}_0} = \frac{1}{\sqrt{2}} \begin{pmatrix} 0 & 0 & \frac{iR_2}{R_2'} & 1 \\ \frac{iR_2'}{R_2} & 1 & 0 & 0 \\ 0 & 0 & -\frac{iR_2}{R_2'} & 1 \\ -\frac{iR_2'}{R_2} & 1 & 0 & 0 \end{pmatrix}$$

and

$$U_{\mathbf{A}_0}\mathbf{A}_0 U_{\mathbf{A}_0}^{-1} = \begin{pmatrix} -iR_2' + \Delta & 0 & 0 & 0 \\ 0 & -iR_2' + \Delta & 0 & 0 \\ 0 & 0 & iR_2' + \Delta & 0 \\ 0 & 0 & 0 & iR_2' + \Delta \end{pmatrix},$$

where $R_2' = \sqrt{R_2^2 + R_1 R_2 S_0}$.

Diagonalization of $\mathbf{A}$ may be carried out without affecting $\mathbf{H}$, and likewise $\mathbf{H}$ may be diagonalized independently of $\mathbf{A}$. This commutivity exists because the structure of $\mathbf{A}$ has been simplified considerably by the assumption $S_n = S_0$, and $\mathbf{A}$ consists of the sub-matrix $\mathbf{A}_0$ repeated on the diagonal of $\mathbf{A}$. Furthermore, $\mathbf{H}$ consists of 4×4 identity matrices repeated along sub- and super-diagonals.In summary:

$$\begin{aligned}[\mathbf{A}+\mathbf{H}] &= U_{\mathbf{H}}U_{\mathbf{A}}(\mathbf{A}+\mathbf{H})U_{\mathbf{A}}^{-1}U_{\mathbf{H}}^{-1} \\ &= U_{\mathbf{A}}U_{\mathbf{H}}(\mathbf{A}+\mathbf{H})U_{\mathbf{H}}^{-1}U_{\mathbf{A}}^{-1} = [\mathbf{A}]+[\mathbf{H}],\end{aligned}$$

where [ ] denotes the diagonal frame of a matrix. Now, $[\mathbf{A}]+\mathbf{H}$ behaves as a set of four decoupled uniform tri-diagonal matrices, and the eigenvalues of $[\mathbf{A}]+\mathbf{H}$ are the sum of the eigenvalues of $\mathbf{A}$ and $\mathbf{H}$. The diagonalizing matrix of $\mathbf{H}$ (for any finite truncation) may be written in sub-blocks consisting of the 4×4 unit matrix multiplied by the tri-diagonal eigenvector element common to all four decoupled tri-diagonal matrices. The eigenvalues and eigenvectors of a uniform tri-diagonal matrix are trigonometric, with trigonometric eigenvalues [24]. A finite truncation of the matrix necessitates boundary conditions; these fix both the eigenvectors and eigenvalues such that they may be indexed by two numbers (the infinite matrix itself, considered in an l_∞ banach space has a uncountable set of eigenvalues and eigen vectors). Here, the indices have been written to conform with the enumeration of the harmonics.

$$U_{\mathbf{H}} = \begin{pmatrix} \ddots & & \vdots & & \iddots \\ & v_{-1,-1}\cdot I_4 & v_{-1,0}\cdot I_4 & v_{-1,1}\cdot I_4 & \\ \cdots & v_{0,-1}\cdot I_4 & v_{0,0}\cdot I_4 & v_{0,1}\cdot I_4 & \cdots \\ & v_{1,-1}\cdot I_4 & v_{1,0}\cdot I_4 & v_{1,1}\cdot I_4 & \\ \iddots & & \vdots & & \ddots \end{pmatrix}, \tag{A.6}$$

where I_4 is the 4×4 identity matrix.For a truncation that contains harmonics up to $\pm N$, the elements are: $v_{n,m} = \frac{1}{\sqrt{N+1}} \sin\left(\frac{\pi}{2(N+1)}\cdot(N+1-n)\cdot(N+1-m)\right)$. The columns are eigenvectors of $\mathbf{H}$ with the eigenvalues $\frac{\gamma h_m}{2}\sin\left(\frac{\pi}{2(N+1)}n\right)$. The inverse of $U_{\mathbf{H}}$ is simply given by transposition [24].We now compute:

$$(\mathbf{A}+\mathbf{H})^{-1} = U_{\mathbf{H}}^{-1}U_{\mathbf{A}}^{-1}\frac{1}{[\mathbf{A}]+[\mathbf{H}]}U_{\mathbf{A}}U_{\mathbf{H}}.$$

Evaluation of of $U_{\mathbf{A}}^{-1}\frac{1}{[\mathbf{A}]+[\mathbf{H}]}U_{\mathbf{A}}$ is as follows:

$$\frac{1}{[\mathbf{A}]+[\mathbf{H}]} = \begin{pmatrix} \ddots & 0 & 0 & 0 & 0 & \iddots \\ 0 & \boxed{\frac{1}{\alpha_k}} & 0 & 0 & 0 & 0 \\ 0 & 0 & \frac{1}{\alpha_k} & 0 & 0 & 0 \\ 0 & 0 & 0 & \frac{1}{\beta_k} & 0 & 0 \\ 0 & 0 & 0 & 0 & \underline{\frac{1}{\beta_k}} & 0 \\ \iddots & 0 & 0 & 0 & 0 & \ddots \end{pmatrix}, \tag{A.7}$$

$$\frac{1}{\alpha_k} = \frac{1}{-iR_2' + \Delta + \frac{\gamma h_m}{2}\sin\left(\frac{k\pi}{2N+2}\right)},$$

$$\frac{1}{\beta_k} = \frac{1}{iR_2' + \Delta + \frac{\gamma h_m}{2}\sin\left(\frac{k\pi}{2N+2}\right)},$$

where k is the index which labels the unique tri-diagonal eigenvector elements v, and N is the largest index for a finite truncation of $\mathbf{A}+\mathbf{H}$. By direct computation using $U_{\mathbf{A}}$:

$$U_{\mathbf{A}}^{-1}\frac{1}{[\mathbf{A}]+[\mathbf{H}]}U_{\mathbf{A}} = \begin{pmatrix} \ddots & 0 & 0 & 0 & 0 & \iddots \\ 0 & \boxed{\frac{1}{2}\left(\frac{1}{\alpha_k}+\frac{1}{\beta_k}\right)} & -\frac{i}{2}\frac{R_2}{R_2'}\left(\frac{1}{\alpha_k}-\frac{1}{\beta_k}\right) & 0 & 0 & 0 \\ 0 & \frac{i}{2}\frac{R_2'}{R_2}\left(\frac{1}{\alpha_k}-\frac{1}{\beta_k}\right) & \frac{1}{2}\left(\frac{1}{\alpha_k}+\frac{1}{\beta_k}\right) & 0 & 0 & 0 \\ 0 & 0 & 0 & \frac{1}{2}\left(\frac{1}{\alpha_k}+\frac{1}{\beta_k}\right) & -\frac{1}{2}\frac{R_2'}{R_2}\left(\frac{1}{\alpha_k}-\frac{1}{\beta_k}\right) & 0 \\ 0 & 0 & 0 & \frac{i}{2}\frac{R_2}{R_2'}\left(\frac{1}{\alpha_k}-\frac{1}{\beta_k}\right) & \underline{\frac{1}{2}\left(\frac{1}{\alpha_k}+\frac{1}{\beta_k}\right)} & 0 \\ \iddots & 0 & 0 & 0 & 0 & \ddots \end{pmatrix} \tag{A.8}$$

$(\mathbf{A}+\mathbf{H})^{-1}$ now has the following form, letting $\mathbf{M}_k$ represent the 4×4 sub-matrices of (A.8) and using $U_{\mathbf{H}}$:

$$(\mathbf{A}+\mathbf{H})^{-1} = U_{\mathbf{H}}^{-1}\begin{pmatrix} \ddots & 0 & 0 & 0 & \iddots \\ 0 & \mathbf{M}_{-1} & 0 & 0 & 0 \\ 0 & 0 & \mathbf{M}_0 & 0 & 0 \\ 0 & 0 & 0 & \mathbf{M}_1 & 0 \\ \iddots & 0 & 0 & 0 & \ddots \end{pmatrix} U_{\mathbf{H}}.$$

Using the form of $U_{\mathbf{H}}$, (A.6), the general 4×4 sub-matrix $(\mathbf{i},\mathbf{j})$ of $(\mathbf{A}+\mathbf{H})^{-1}$ that results from this multiplication is given by:

$$(\mathbf{A}+\mathbf{H})^{-1}_{\mathbf{i},\mathbf{j}} = \sum_{-N}^{N} v_{\mathbf{i},n}\mathbf{M}_n v_{n,\mathbf{j}}.$$

For truncation of the matrix at the Nth harmonic this sum is:

$$(\mathbf{A}+\mathbf{H})^{-1}_{\mathbf{i},\mathbf{j}} = \frac{1}{N+1}\sum_{-N}^{N}\sin\left(\frac{\pi}{2(N+1)}\cdot(N+1-\mathbf{i})\cdot(N+1-n)\right)\mathbf{M}_n\left(\frac{\gamma h_{\mathrm{m}}}{2}\sin\left(\frac{n\pi}{2N+2}\right)\right)\times\sin\left(\frac{\pi}{2(N+1)}\cdot(N+1-n)\cdot(N+1-\mathbf{j})\right).$$

This expression, using the functions defined by $\mathbf{M}$, gives all of the signals up to the Nth harmonic to zero order in ω_{m}. The signals to zero order are obtained as $\chi = (\mathbf{A}+\mathbf{H})^{-1}\cdot\mathbf{Z}_0$ (see (A.5)). The equilibrium solution $\mathbf{Z}_0$ on the right hand side selects only the column containing the $\mathbf{j}=0$, 4×4 sub-matrices. The signals are thus given by:

$$\chi_{\mathbf{i}} = \frac{1}{N+1}\sum_{-N}^{N}\sin\left(\frac{\pi}{2(N+1)}\cdot(N+1-\mathbf{i})\cdot(N+1-n)\right)\times\mathbf{M}_n\left(\frac{\gamma h_{\mathrm{m}}}{2}\sin\left(\frac{n\pi}{2N+2}\right)\right)\sin\left(\frac{\pi}{2}\cdot(N+1-n)\right).$$

Shifting the summation index by $N+1$ and using trigonometric identities:

$$\chi_{\mathbf{i}} = \frac{1}{N+1}\sum_{1}^{2N+1}\frac{1}{2}(1-\cos(n\pi))\cos\left(\frac{\pi n\mathbf{i}}{2(N+1)}\right)\times\mathbf{M}_n\left(\frac{\gamma h_{\mathrm{m}}}{2}\cos\left(\frac{n\pi}{2N+2}\right)\right). \tag{A.9}$$

The term $(1-\cos(n\pi))$ eliminates the even points of summation. The only dependence of $\mathbf{M}_n$ on the index n is through the modulation term, the functional form of the $\mathbf{M}_n$ is the same otherwise. So that, in the limit as $N\uparrow\infty$:

$$\chi_{\mathbf{i}} = \frac{1}{\pi}\int_0^{\pi}\cos(\mathbf{i}\theta)\mathbf{M}\left(\frac{\gamma h_{\mathrm{m}}}{2}\cos(\theta)\right)\mathrm{d}\theta. \tag{A.10}$$

Eq. (A.10) is of the form of (1) in the main text. Expression of $\mathbf{M}$ as the Fourier transform of a function in the time domain will reveal the Bessel function dependence χ_i. All the nonzero elements of the matrix $\mathbf{M}$ are the real or imaginary components of the basic complex Lorentzian lineshape $1/(\Delta+\frac{\gamma h_{\mathrm{m}}}{2}\cos(\theta)+\mathrm{i}R_2')$ (see (A.7)).

In-phase signals are, therefore, given by:

$$\chi_{\mathbf{i}}(\Delta) \propto \int_0^{\infty}\mathrm{e}^{-R_2' t}\left[\frac{1}{\pi}\int_0^{\pi}\cos(\mathbf{i}\theta)\mathrm{e}^{\mathrm{i}\cdot\left(\frac{\gamma h_{\mathrm{m}}}{2}\cos(\theta)\right)\cdot t}\,\mathrm{d}\theta\right]\times\begin{pmatrix}\cos(\Delta\cdot t)\\ \sin(\Delta\cdot t)\end{pmatrix}\mathrm{d}t.$$

But,

$$J_n\left(\frac{h_{\mathrm{m}}}{2}t\right) = \begin{pmatrix}\mathrm{Re}\\ \mathrm{Im}\end{pmatrix}^{n\,\mathrm{even}}_{n\,\mathrm{odd}}\left(\frac{(\mathrm{i})^n}{\pi}\int_0^{\pi}\cos(n\cdot\theta)\mathrm{e}^{\mathrm{i}\cdot\left(\frac{\gamma h_{\mathrm{m}}}{2}t\right)\cos(\theta)}\,\mathrm{d}\theta\right). \tag{A.11}$$

(See Watson, Treatise on Bessel functions [15, p. 21 Eqs. (8) and (9)], these two equations are combine by extending the integration range from $\pi/2$ to π). The contribution (A.11) to the integral (A.10) was tested against the discrete sum (A.9) numerically in Matlab using the built-in Bessel functions [19].This gives the form required by pseudo-modulation (see Eq. (4)):

$$\chi_{\mathbf{i}}(\Delta) \propto \int_0^{\infty}\mathrm{e}^{-R_2' t}J_n\left(\frac{\gamma h_{\mathrm{m}}}{2}t\right)\begin{pmatrix}\cos(\Delta\cdot t)\\ \sin(\Delta\cdot t)\end{pmatrix}\mathrm{d}t.$$

To calculate the quadrature signals to first order in modulation frequency, all of the summed expressions $(\mathbf{A}+\mathbf{H})^{-1}_{\mathbf{i},\mathbf{j}} = \sum_{-N}^{N} v_{\mathbf{i},n}\mathbf{M}_n v_{n,\mathbf{j}}$ must be calculated because is it is the zeroth harmonic column of the perturbation term $(\mathbf{A}+\mathbf{H})^{-1}\cdot\mathbf{W}\cdot(\mathbf{A}+\mathbf{H})^{-1}$ that will be selected by $\mathbf{Z}_0$, to give the quadrature signals (see (A.5)). The general elements $(\mathbf{A}+\mathbf{H})^{-1}_{\mathbf{i},\mathbf{j}}$ may be calculated in analogy to the derivation above.

$$\begin{aligned}\lim_{N\to\infty}(\mathbf{A}+\mathbf{H})^{-1}_{\mathbf{i},\mathbf{j}} &= \frac{1}{\pi}\int_0^{\pi}\cos(\mathbf{i}\theta)\cos(\mathbf{j}\theta)\mathbf{M}\left(\frac{\gamma h_{\mathrm{m}}}{2}\cos(\theta)\right)\mathrm{d}\theta\\ &\quad+\frac{1}{\pi}\int_0^{\pi}\sin(\mathbf{i}\theta)\sin(\mathbf{j}\theta)\mathbf{M}\left(\frac{\gamma h_{\mathrm{m}}}{2}\cos(\theta)\right)\mathrm{d}\theta\\ &= \frac{1}{\pi}\int_0^{\pi}\cos((\mathbf{i}-\mathbf{j})\theta)\mathbf{M}\left(\frac{\gamma h_{\mathrm{m}}}{2}\cos(\theta)\right)\mathrm{d}\theta.\end{aligned}$$

The procedure of passing to the conjugate Fourier space that was used above shows that the general 4×4 sub-matrices of $(\mathbf{A}+\mathbf{H})^{-1}$ are thus just sin and cos components of the Bessel–Fourier integral transform of a simple exponential function with R_2' rate. The order of the Bessel function in each sub-matrix is $\mathbf{i}-\mathbf{j}$.

The structure of $(\mathbf{A}+\mathbf{H})^{-1}$ can explicitly be displayed. Note that the notation adopted here should not be confused with final absorption and dispersion line shapes, but is chosen here to emphasize the subcomponents that make these up. The use of primed letters in the definition of the matrix elements of $(\mathbf{A}+\mathbf{H})^{-1}$ should not be confused with the similar notation for quadrature signals.

$$(\mathbf{A}+\mathbf{H})^{-1}=\begin{pmatrix}
\ddots & & & & & & & & & & & \iddots\\
& \boxed{\mathrm{D}_0} & \mathrm{A}_0 & 0 & 0 & \boxed{\mathrm{D}_{-1}} & \mathrm{A}_{-1} & 0 & 0 & \boxed{\mathrm{D}_{-2}} & \mathrm{A}_{-2} & 0 & 0\\
& -\mathrm{A}'_0 & \mathrm{D}_0 & 0 & 0 & -\mathrm{A}'_{-1} & \mathrm{D}_{-1} & 0 & 0 & -\mathrm{A}'_{-2} & \mathrm{D}_{-2} & 0 & 0\\
& 0 & 0 & \mathrm{D}_0 & \mathrm{A}'_0 & 0 & 0 & \mathrm{D}_{-1} & \mathrm{A}'_{-1} & 0 & 0 & \mathrm{D}_{-2} & \mathrm{A}'_{-2}\\
& 0 & 0 & -\mathrm{A}_0 & \underline{\mathrm{D}_0} & 0 & 0 & -\mathrm{A}_{-1} & \underline{\mathrm{D}_{-1}} & 0 & 0 & -\mathrm{A}_{-2} & \underline{\mathrm{D}_{-2}}\\
& \boxed{\mathrm{D}_1} & \mathrm{A}_1 & 0 & 0 & \boxed{\mathrm{D}_0} & \mathrm{A}_0 & 0 & 0 & \boxed{\mathrm{D}_{-1}} & \mathrm{A}_{-1} & 0 & 0\\
& -\mathrm{A}'_1 & \mathrm{D}_1 & 0 & 0 & -\mathrm{A}'_0 & \mathrm{D}_0 & 0 & 0 & -\mathrm{A}'_{-1} & \mathrm{D}_{-1} & 0 & 0\\
& 0 & 0 & \mathrm{D}_1 & \mathrm{A}'_1 & 0 & 0 & \mathrm{D}_0 & \mathrm{A}'_0 & 0 & 0 & \mathrm{D}_{-1} & \mathrm{A}'_{-1}\\
& 0 & 0 & -\mathrm{A}_1 & \underline{\mathrm{D}_1} & 0 & 0 & -\mathrm{A}_0 & \underline{\mathrm{D}_0} & 0 & 0 & -\mathrm{A}_{-1} & \underline{\mathrm{D}_{-1}}\\
& \boxed{\mathrm{D}_2} & \mathrm{A}_2 & 0 & 0 & \boxed{\mathrm{D}_1} & \mathrm{A}_1 & 0 & 0 & \boxed{\mathrm{D}_0} & \mathrm{A}_0 & 0 & 0\\
& -\mathrm{A}'_2 & \mathrm{D}_2 & 0 & 0 & -\mathrm{A}'_1 & \mathrm{D}_1 & 0 & 0 & -\mathrm{A}'_0 & \mathrm{D}_0 & 0 & 0\\
& 0 & 0 & \mathrm{D}_2 & \mathrm{A}'_2 & 0 & 0 & \mathrm{D}_1 & \mathrm{A}'_1 & 0 & 0 & \mathrm{D}_0 & \mathrm{A}'_0\\
& 0 & 0 & -\mathrm{A}_2 & \underline{\mathrm{D}_2} & 0 & 0 & -\mathrm{A}_1 & \underline{\mathrm{D}_1} & 0 & 0 & -\mathrm{A}_0 & \underline{\mathrm{D}_0}\\
\iddots & & & & & & & & & & & & \ddots
\end{pmatrix},$$

where

$$\begin{aligned}
\mathrm{A}_n &= -\frac{\mathrm{i}}{2}\frac{R_2}{R'_2}\frac{1}{\pi}\int_0^{\pi}\cos(n\theta)\\
&\quad\times\left(\frac{1}{-\mathrm{i}R'_2+\Delta+\frac{\gamma h_\mathrm{m}}{2}\cos(\theta)}-\frac{1}{\mathrm{i}R'_2+\Delta+\frac{\gamma h_\mathrm{m}}{2}\cos(\theta)}\right)\mathrm{d}\theta\\
&=\frac{R_2}{R'_2}\frac{1}{\pi}\int_0^{\pi}\cos(n\theta)\\
&\quad\times\int_0^{\infty}\mathrm{e}^{-R'_2t}\frac{\mathrm{e}^{\mathrm{i}\cdot\left(\Delta+\frac{\gamma h_\mathrm{m}}{2}\cos(\theta)\right)\cdot t}+\mathrm{e}^{-\mathrm{i}\cdot\left(\Delta+\frac{\gamma h_\mathrm{m}}{2}\cos(\theta)\right)\cdot t}}{2}\mathrm{d}t\mathrm{d}\theta\\
&=\frac{(\mathrm{i})^n}{2}\frac{R_2}{R'_2}\int_{-\infty}^{\infty}\mathrm{e}^{-R'_2|t|}J_n\left(\frac{\gamma h_\mathrm{m}}{2}t\right)\mathrm{e}^{\mathrm{i}\cdot\Delta\cdot t}\mathrm{d}t,
\end{aligned}$$

$$\boxed{\mathrm{A}_n=(\mathrm{i})^n\frac{R_2}{R'_2}\int_0^{\infty}\mathrm{e}^{-R'_2t}J_n\left(\tfrac{\gamma h_\mathrm{m}}{2}t\right)\begin{pmatrix}\cos(\Delta\cdot t)\\ \mathrm{i}\cdot\sin(\Delta\cdot t)\end{pmatrix}_{n\,\mathrm{odd}}^{n\,\mathrm{even}}\mathrm{d}t.}\tag{A.12}$$

A'_n is formed from A_n by $R_2/R'_2\rightarrow R'_2/R_2$ in the prefactor of the integral.

$$\begin{aligned}
\mathrm{D}_n &= \frac{1}{2}\frac{1}{\pi}\int_0^{\pi}\cos(n\theta)\\
&\quad\times\left(\frac{1}{-\mathrm{i}R'_2+\Delta+\frac{\gamma h_\mathrm{m}}{2}\cos(\theta)}+\frac{1}{\mathrm{i}R'_2+\Delta+\frac{\gamma h_\mathrm{m}}{2}\cos(\theta)}\right)\mathrm{d}\theta\\
&=\frac{1}{\pi}\int_0^{\pi}\cos(n\theta)\\
&\quad\times\int_0^{\infty}\mathrm{e}^{-R'_2t}\frac{\mathrm{e}^{\mathrm{i}\cdot\left(\Delta+\frac{\gamma h_\mathrm{m}}{2}\cos(\theta)\right)\cdot t}-\mathrm{e}^{-\mathrm{i}\cdot\left(\Delta+\frac{\gamma h_\mathrm{m}}{2}\cos(\theta)\right)\cdot t}}{2\mathrm{i}}\mathrm{d}t\mathrm{d}\theta,
\end{aligned}$$

$$\boxed{\mathrm{D}_n=(\mathrm{i})^n\int_0^{\infty}\mathrm{e}^{-R'_2t}J_n\left(\tfrac{\gamma h_\mathrm{m}}{2}t\right)\begin{pmatrix}\sin(\Delta\cdot t)\\ -\mathrm{i}\cdot\cos(\Delta\cdot t)\end{pmatrix}_{n\,\mathrm{odd}}^{n\,\mathrm{even}}\mathrm{d}t.}\tag{A.13}$$

The 4×4 sub matrices of $(\mathbf{A}+\mathbf{H})^{-1}\cdot\mathbf{W}\cdot(\mathbf{A}+\mathbf{H})^{-1}$ may be written as the summation:

$$\begin{aligned}
&\left((\mathbf{A}+\mathbf{H})^{-1}\cdot\mathbf{W}\cdot(\mathbf{A}+\mathbf{H})^{-1}\right)_{\mathbf{i},\mathbf{j}}\\
&\quad=\sum_n\begin{pmatrix}\mathrm{D}_{\mathbf{i}-n} & \mathrm{A}_{\mathbf{i}-n} & 0 & 0\\ -\mathrm{A}'_{\mathbf{i}-n} & \mathrm{D}_{\mathbf{i}-n} & 0 & 0\\ 0 & 0 & \mathrm{D}_{\mathbf{i}-n} & \mathrm{A}'_{\mathbf{i}-n}\\ 0 & 0 & -\mathrm{A}_{\mathbf{i}-n} & \mathrm{D}_{\mathbf{i}-n}\end{pmatrix}\\
&\qquad\times\begin{pmatrix}0 & 0 & n\omega_\mathrm{m} & 0\\ 0 & 0 & 0 & n\omega'_\mathrm{m}\\ n\omega'_\mathrm{m} & 0 & 0 & 0\\ 0 & n\omega_\mathrm{m} & 0 & 0\end{pmatrix}\\
&\qquad\times\begin{pmatrix}\mathrm{D}_{n-\mathbf{j}} & \mathrm{A}_{n-\mathbf{j}} & 0 & 0\\ -\mathrm{A}'_{n-\mathbf{j}} & \mathrm{D}_{n-\mathbf{j}} & 0 & 0\\ 0 & 0 & \mathrm{D}_{n-\mathbf{j}} & \mathrm{A}'_{n-\mathbf{j}}\\ 0 & 0 & -\mathrm{A}_{n-\mathbf{j}} & \mathrm{D}_{n-\mathbf{j}}\end{pmatrix},
\end{aligned}$$

where $n\omega'_\mathrm{m}=n\omega_\mathrm{m}(1-S_0)$

$$=\sum_n n\begin{pmatrix}0 & \mathcal{Q}'_n\\ \mathcal{Q}_n & 0\end{pmatrix}$$

$$\mathcal{Q}_n=\begin{pmatrix}\omega'_\mathrm{m}\mathrm{D}_{\mathbf{i}-n}\mathrm{D}_{n-\mathbf{j}}-\omega_\mathrm{m}\mathrm{A}'_{\mathbf{i}-n}\mathrm{A}'_{n-\mathbf{j}} & \omega'_\mathrm{m}\mathrm{D}_{\mathbf{i}-n}\mathrm{A}_{n-\mathbf{j}}+\omega_\mathrm{m}\mathrm{A}'_{\mathbf{i}-n}\mathrm{D}_{n-\mathbf{j}}\\ -\omega'_\mathrm{m}\mathrm{A}_{\mathbf{i}-n}\mathrm{D}_{n-\mathbf{j}}-\omega_\mathrm{m}\mathrm{D}_{\mathbf{i}-n}\mathrm{A}'_{n-\mathbf{j}} & -\omega'_\mathrm{m}\mathrm{A}_{\mathbf{i}-n}\mathrm{A}_{n-\mathbf{j}}+\omega_\mathrm{m}\mathrm{D}_{\mathbf{i}-n}\mathrm{D}_{n-\mathbf{j}}\end{pmatrix},$$

$$\mathcal{Q}'_n=\begin{pmatrix}\omega_\mathrm{m}\mathrm{D}_{\mathbf{i}-n}\mathrm{D}_{n-\mathbf{j}}-\omega'_\mathrm{m}\mathrm{A}_{\mathbf{i}-n}\mathrm{A}_{n-\mathbf{j}} & \omega_\mathrm{m}\mathrm{D}_{\mathbf{i}-n}\mathrm{A}'_{n-\mathbf{j}}+\omega'_\mathrm{m}\mathrm{A}_{\mathbf{i}-n}\mathrm{D}_{n-\mathbf{j}}\\ -\omega_\mathrm{m}\mathrm{A}'_{\mathbf{i}-n}\mathrm{D}_{n-\mathbf{j}}-\omega'_\mathrm{m}\mathrm{D}_{\mathbf{i}-n}\mathrm{A}_{n-\mathbf{j}} & -\omega_\mathrm{m}\mathrm{A}'_{\mathbf{i}-n}\mathrm{A}'_{n-\mathbf{j}}+\omega'_\mathrm{m}\mathrm{D}_{\mathbf{i}-n}\mathrm{D}_{n-\mathbf{j}}\end{pmatrix}.$$

When $\mathbf{Z}_0$ is applied to $(\mathbf{A}+\mathbf{H})^{-1}(\mathbf{A}+\mathbf{H})^{-1}\cdot\mathbf{W}\cdot(\mathbf{A}+\mathbf{H})^{-1}$, the quadrature signals are:

$$-\mathrm{Abs}'_{\mathbf{i}}(\Delta)=\sum_n\left(\omega'_{\mathrm{m}}\mathbf{A}_{\mathbf{i}-n}\mathbf{A}_n-\omega_{\mathrm{m}}\mathbf{D}_{\mathbf{i}-n}\mathbf{D}_n\right)$$

and

$$\mathrm{Disp}'_{\mathbf{i}}(\Delta)=-\sum_n\left(\omega'_{\mathrm{m}}\mathbf{D}_{\mathbf{i}-n}\mathbf{A}_n+\omega_{\mathrm{m}}\mathbf{A}'_{\mathbf{i}-n}\mathbf{D}_n\right).$$

Taking *non-saturated* absorption as a first example, the definitions in terms of integrals over Bessel functions may be substituted. If saturation is negligible for both the ω'_{m} and R'_2 terms then:

$$\begin{aligned}-\mathrm{Abs}'_{\mathbf{i}}(\Delta)&=-A'_{\mathbf{i}}(\Delta)\\&=(\mathrm{i})^{\mathbf{i}}\omega_{\mathrm{m}}\cdot\sum_n n\left(\int_0^\infty\int_0^\infty \mathrm{e}^{-R_2(t_1+t_2)}J_{\mathbf{i}-n}\left(\frac{\gamma h_{\mathrm{m}}}{2}t_1\right)\right.\\&\quad\times J_n\left(\frac{\gamma h_{\mathrm{m}}}{2}t_2\right)\begin{pmatrix}\cos(\Delta\cdot t_1)\\ \mathrm{i}\sin(\Delta\cdot t_1)\end{pmatrix}^{\mathbf{i}-n\,\mathrm{even}}_{\mathbf{i}-n\,\mathrm{odd}}\\&\quad\times\begin{pmatrix}\cos(\Delta\cdot t_2)\\ \mathrm{i}\sin(\Delta\cdot t_2)\end{pmatrix}^{n\,\mathrm{even}}_{n\,\mathrm{odd}}\mathrm{d}t_1\,\mathrm{d}t_2-\int_0^\infty\int_0^\infty \mathrm{e}^{-R_2(t_1+t_2)}\\&\quad\times J_{\mathbf{i}-n}\left(\frac{\gamma h_{\mathrm{m}}}{2}t_1\right)J_n\left(\frac{\gamma h_{\mathrm{m}}}{2}t_2\right)\begin{pmatrix}\sin(\Delta\cdot t_1)\\ -\mathrm{i}\cos(\Delta\cdot t_1)\end{pmatrix}^{\mathbf{i}-n\,\mathrm{even}}_{\mathbf{i}-n\,\mathrm{odd}}\\&\quad\left.\times\begin{pmatrix}\sin(\Delta\cdot t_2)\\ -\mathrm{i}\cos(\Delta\cdot t_2)\end{pmatrix}^{n\,\mathrm{even}}_{n\,\mathrm{odd}}\mathrm{d}t_1\,\mathrm{d}t_2\right).\end{aligned}$$

For the case $\mathbf{i}$ is even, then $(\mathbf{i}-n)$ even (odd) iff n even (odd). For $\mathbf{i}$ odd then $(\mathbf{i}-n)$ even (odd) iff n odd (even).

$$\begin{aligned}-A'_{\mathbf{i}}(\Delta)&=(\mathrm{i})^{\mathbf{i}}\omega_{\mathrm{m}}\int_0^\infty\int_0^\infty \mathrm{e}^{-R_2(t_1+t_2)}\\&\quad\times\sum_n n\left(J_{\mathbf{i}-n}\left(\frac{h_{\mathrm{m}}}{2}t_1\right)J_n\left(\frac{h_{\mathrm{m}}}{2}t_2\right)\right)\\&\quad\times\begin{pmatrix}\cos(\Delta\cdot(t_1+t_2))\\ \mathrm{i}\cdot\sin(\Delta\cdot(t_1+t_2))\end{pmatrix}^{\mathbf{i}\,\mathrm{even}}_{\mathbf{i}\,\mathrm{odd}}\mathrm{d}t_1\,\mathrm{d}t_2.\end{aligned}$$

To evaluate $\sum_n n(J_{\mathbf{i}-n}(\frac{\gamma h_{\mathrm{m}}}{2}t_1)J_n(\frac{\gamma h_{\mathrm{m}}}{2}t_2))$ the limit as $N\uparrow\infty$ is applied, so that the sum is over all positive and negative n. Then use the recurrence relation for Bessel functions, $J_{n+1}(z)+J_{n-1}(z)=\frac{2n}{z}J_n(z)$ and $\sum_n J_n(z_1)J_{m-n}(z_2)=J_m(z_1+z_2)$ [15]:

$$\begin{aligned}-A'_{\mathbf{i}}(\Delta)&=(\mathrm{i})^{\mathbf{i}}\omega_{\mathrm{m}}\int_0^\infty\int_0^\infty \mathrm{e}^{-R_2(t_1+t_2)}\left(\frac{\mathbf{i}\cdot t_2}{t_1+t_2}\right)J_{\mathbf{i}}\left(\frac{\gamma h_{\mathrm{m}}}{2}(t_1+t_2)\right)\\&\quad\times\begin{pmatrix}\cos(\Delta\cdot(t_1+t_2))\\ \mathrm{i}\cdot\sin(\Delta\cdot(t_1+t_2))\end{pmatrix}^{\mathbf{i}\,\mathrm{even}}_{\mathbf{i}\,\mathrm{odd}}\mathrm{d}t_1\,\mathrm{d}t_2\\&=\mathbf{i}\cdot(\mathrm{i})^{\mathbf{i}}\omega_{\mathrm{m}}\int_0^\infty t_2\int_{t_2}^\infty \mathrm{e}^{-R_2t}\left(\frac{1}{t}\right)J_{\mathbf{i}}\left(\frac{\gamma h_{\mathrm{m}}}{2}t\right)\\&\quad\times\begin{pmatrix}\cos(\Delta\cdot t)\\ \mathrm{i}\cdot\sin(\Delta\cdot t)\end{pmatrix}^{\mathbf{i}\,\mathrm{even}}_{\mathbf{i}\,\mathrm{odd}}\mathrm{d}t\,\mathrm{d}t_2.\end{aligned}$$

Integrating by parts:

$$=\mathbf{i}\cdot(\mathrm{i})^{\mathbf{i}}\omega_{\mathrm{m}}\int_0^\infty\frac{t}{2}\cdot\mathrm{e}^{-R_2t}J_{\mathbf{i}}\left(\frac{\gamma h_{\mathrm{m}}}{2}t\right)\begin{pmatrix}\cos(\Delta\cdot t)\\ \mathrm{i}\cdot\sin(\Delta\cdot t)\end{pmatrix}^{\mathbf{i}\,\mathrm{even}}_{\mathbf{i}\,\mathrm{odd}}\mathrm{d}t$$

and

$$\begin{aligned}A'_{\mathbf{i}}(\Delta)&=-\mathbf{i}\cdot(\mathrm{i})^{\mathbf{i}}\tfrac{\omega_{\mathrm{m}}}{2}\tfrac{\partial}{\partial\Delta}\textstyle\int_0^\infty \mathrm{e}^{-R_2t}J_{\mathbf{i}}\left(\frac{\gamma h_{\mathrm{m}}}{2}t\right)\\&\quad\times\begin{pmatrix}\sin(\Delta\cdot t)\\ -\mathrm{i}\cdot\cos(\Delta\cdot t)\end{pmatrix}^{\mathbf{i}\,\mathrm{even}}_{\mathbf{i}\,\mathrm{odd}}\mathrm{d}t\\&=-\frac{\mathbf{i}\omega_{\mathrm{m}}}{2}\frac{\partial}{\partial\Delta}D_{\mathbf{i}}(\Delta).\end{aligned}$$

Likewise

$$\begin{aligned}D'_{\mathbf{i}}(\Delta)&=-\mathbf{i}\cdot(\mathrm{i})^{\mathbf{i}}\omega_{\mathrm{m}}\textstyle\int_0^\infty t_2\int_{t_2}^\infty \mathrm{e}^{-R_2t}\left(\frac{1}{t}\right)J_{\mathbf{i}}\left(\frac{\gamma h_{\mathrm{m}}}{2}t\right)\\&\quad\times\begin{pmatrix}\sin(\Delta\cdot t)\\ -\mathrm{i}\cdot\cos(\Delta\cdot t)\end{pmatrix}^{\mathbf{i}\,\mathrm{even}}_{\mathbf{i}\,\mathrm{odd}}\mathrm{d}t\,\mathrm{d}t_2\end{aligned}$$

and

$$\begin{aligned}D'_{\mathbf{i}}(\Delta)&=\mathbf{i}\cdot(\mathrm{i})^{\mathbf{i}}\tfrac{\omega_{\mathrm{m}}}{2}\tfrac{\partial}{\partial\Delta}\textstyle\int_0^\infty \mathrm{e}^{-R_2t}J_{\mathbf{i}}\left(\frac{\gamma h_{\mathrm{m}}}{2}t\right)\\&\quad\times\begin{pmatrix}\cos(\Delta\cdot t)\\ \mathrm{i}\cdot\sin(\Delta\cdot t)\end{pmatrix}^{\mathbf{i}\,\mathrm{even}}_{\mathbf{i}\,\mathrm{odd}}\mathrm{d}t\\&=\frac{\mathbf{i}\omega_{\mathrm{m}}}{2}\frac{\partial}{\partial\Delta}A_{\mathbf{i}}(\Delta).\end{aligned}$$

These are the answers without saturation, saturation may be included, however, by re-working the above derivation.

$$\begin{aligned}-\mathrm{Abs}'_{\mathbf{i}}(\Delta)&=-A'_{\mathbf{i}}(\Delta)\\&=(\mathrm{i})^{\mathbf{i}}\omega_{\mathrm{m}}\sum_n n\left(K\int_0^\infty\int_0^\infty \mathrm{e}^{-R'_2(t_1+t_2)}J_{\mathbf{i}-n}\left(\frac{\gamma h_{\mathrm{m}}}{2}t_1\right)\right.\\&\quad\times J_n\left(\frac{\gamma h_{\mathrm{m}}}{2}t_2\right)\begin{pmatrix}\cos(\Delta\cdot t_1)\\ \mathrm{i}\sin(\Delta\cdot t_1)\end{pmatrix}^{\mathbf{i}-n\,\mathrm{even}}_{\mathbf{i}-n\,\mathrm{odd}}\\&\quad\times\begin{pmatrix}\cos(\Delta\cdot t_2)\\ \mathrm{i}\sin(\Delta\cdot t_2)\end{pmatrix}^{n\,\mathrm{even}}_{n\,\mathrm{odd}}\mathrm{d}t_1\,\mathrm{d}t_2-\int_0^\infty\int_0^\infty \mathrm{e}^{-R'_2(t_1+t_2)}\\&\quad\times J_{\mathbf{i}-n}\left(\frac{\gamma h_{\mathrm{m}}}{2}t_1\right)J_n\left(\frac{\gamma h_{\mathrm{m}}}{2}t_2\right)\begin{pmatrix}\sin(\Delta\cdot t_1)\\ -\mathrm{i}\cos(\Delta\cdot t_1)\end{pmatrix}^{\mathbf{i}-n\,\mathrm{even}}_{\mathbf{i}-n\,\mathrm{odd}}\\&\quad\left.\times\begin{pmatrix}\sin(\Delta\cdot t_2)\\ -\mathrm{i}\cos(\Delta\cdot t_2)\end{pmatrix}^{n\,\mathrm{even}}_{n\,\mathrm{odd}}\mathrm{d}t_1\,\mathrm{d}t_2\right),\end{aligned}$$

where $K=(1-S_0)\left(\frac{R_2}{R'_2}\right)^2$. It had to be assumed that $n\omega_{\mathrm{m}}\ll R_1$ in the saturation factor (S_n) that had been associated with ω'_{m}. But, this assumption was already made for the saturation factor in the A matrix, so it is in keeping with this previous approximation to assume $S_n\to S_0$ here, as well.

The sums are now broken up into even and odd sums over the Bessel functions because the complement to each even or odd sum is not available from the second

term any longer due to the presence of the saturation constant K.

$$\Sigma_e = \sum_m (2m)\cdot J_{\mathbf{i}-2m}\left(\frac{\gamma h_m}{2}t_1\right)J_{2m}\left(\frac{\gamma h_m}{2}t_2\right),$$

$$\Sigma_o = \sum_m (2m+1)\cdot J_{\mathbf{i}-(2m+1)}\left(\frac{\gamma h_m}{2}t_1\right)J_{2m+1}\left(\frac{\gamma h_m}{2}t_2\right).$$

If $\mathbf{i}$ is even:

$$-A'_{\mathbf{i}}(\Delta) = (\mathrm{i})^{\mathbf{i}}\omega_m\int_0^\infty\int_0^\infty e^{-R'_2(t_1+t_2)} \times\begin{bmatrix} K(\Sigma_e\cdot\cos(\Delta t_1)\cdot\cos(\Delta t_2)+\Sigma_o\cdot-\sin(\Delta t_1)\cdot\sin(\Delta t_2)) \\ -(\Sigma_e\cdot\sin(\Delta t_1)\cdot\sin(\Delta t_2)+\Sigma_o\cdot-\cos(\Delta t_1)\cdot\cos(\Delta t_2))\end{bmatrix}dt_1\,dt_2.$$

If $\mathbf{i}$ is odd:

$$-A'_{\mathbf{i}}(\Delta) = (\mathrm{i})^{\mathbf{i}}\omega_m\int_0^\infty\int_0^\infty e^{-R'_2(t_1+t_2)} \times\begin{bmatrix} K(\Sigma_e\cdot\mathrm{i}\cdot\sin(\Delta t_1)\cdot\cos(\Delta t_2)+\Sigma_o\cdot\mathrm{i}\cdot\cos(\Delta t_1)\cdot\sin(\Delta t_2)) \\ -(\Sigma_e\cdot-\mathrm{i}\cdot\cos(\Delta t_1)\cdot\sin(\Delta t_2)+\Sigma_o\cdot-\mathrm{i}\cdot\sin(\Delta t_1)\cdot\cos(\Delta t_2))\end{bmatrix}dt_1\,dt_2.$$

The even and odd sums may be derived as follows:

$$\Sigma_e+\Sigma_o = \sum_n n\left(J_{\mathbf{i}-n}\left(\frac{\gamma h_m}{2}t_1\right)J_n\left(\frac{\gamma h_m}{2}t_2\right)\right) = \left(\frac{\mathbf{i}\cdot t_2}{t_1+t_2}\right)J_{\mathbf{i}}\left(\frac{\gamma h_m}{2}(t_1+t_2)\right).$$

But, using the symmetry of Bessel functions:

$$\Sigma_e-\Sigma_o = \sum_n n\cdot(-1)^n\left(J_{\mathbf{i}-n}\left(\frac{\gamma h_m}{2}t_1\right)J_n\left(\frac{\gamma h_m}{2}t_2\right)\right) = \sum_n n\cdot\left(J_{\mathbf{i}-n}\left(\frac{\gamma h_m}{2}t_1\right)J_n\left(-\frac{\gamma h_m}{2}t_2\right)\right) = \left(\frac{-\mathbf{i}\cdot t_2}{t_1-t_2}\right)J_{\mathbf{i}}\left(\frac{\gamma h_m}{2}(t_1-t_2)\right).$$

These are applied to give:

$$-A'_{\mathbf{i}}(\Delta) = \mathbf{i}\cdot(\mathrm{i})^{\mathbf{i}}\cdot\omega_m\cdot\int_0^\infty\int_0^\infty e^{-R'_2(t_1+t_2)} \times\left(\frac{(1+K)}{2}\left(\frac{t_2}{t_1+t_2}\right)J_{\mathbf{i}}\left(\frac{\gamma h_m}{2}(t_1+t_2)\right)\cdot\begin{pmatrix}\cos(\Delta(t_1+t_2))\\ \mathrm{i}\cdot\sin(\Delta(t_1+t_2))\end{pmatrix}_{\mathbf{i}\,\mathrm{odd}}^{\mathbf{i}\,\mathrm{even}}+\frac{(1-K)}{2}\left(\frac{t_2}{t_1-t_2}\right)\times J_{\mathbf{i}}\left(\frac{\gamma h_m}{2}(t_1-t_2)\right)\cdot\begin{pmatrix}\cos(\Delta(t_1-t_2))\\ \mathrm{i}\cdot\sin(\Delta(t_1-t_2))\end{pmatrix}_{\mathbf{i}\,\mathrm{odd}}^{\mathbf{i}\,\mathrm{even}}\right)dt_1\,dt_2.$$

The first integral is just the term considered above (in the calculation without saturation), and the result may be substituted immediately. Changing variables in the second integral gives:

$$\frac{(1-K)}{2}\cdot\int_0^\infty t_2e^{-2R'_2t_2}\int_{-\infty}^{t_2}e^{+R'_2t}\frac{-1}{t}J_{\mathbf{i}}\left(\frac{\gamma h_m}{2}t\right)\cdot\begin{pmatrix}\cos(\Delta t)\\ \mathrm{i}\cdot\sin(\Delta t)\end{pmatrix}_{\mathbf{i}\,\mathrm{odd}}^{\mathbf{i}\,\mathrm{even}}dt\,dt_2. \tag{A.14}$$

Now integrate by parts:

$$=\frac{(1-K)}{2}\cdot\left(\frac{1}{(2R'_2)^2}\int_{-\infty}^0 e^{+R'_2t}\frac{-1}{t}J_{\mathbf{i}}\left(\frac{\gamma h_m}{2}t\right)\cdot\begin{pmatrix}\cos(\Delta t)\\ \mathrm{i}\cdot\sin(\Delta t)\end{pmatrix}_{\mathbf{i}\,\mathrm{odd}}^{\mathbf{i}\,\mathrm{even}}dt-\int_0^\infty\left(\frac{te^{-2R'_2t}}{-2R'_2}-\frac{e^{-2R'_2t}}{(2R'_2)^2}\right)e^{+R'_2t}\frac{-1}{t}\times J_{\mathbf{i}}\left(\frac{\gamma h_m}{2}t\right)\cdot\begin{pmatrix}\cos(\Delta t)\\ \mathrm{i}\cdot\sin(\Delta t)\end{pmatrix}_{\mathbf{i}\,\mathrm{odd}}^{\mathbf{i}\,\mathrm{even}}dt\right).$$

Using the symmetry of Bessel functions under sign the boundary term from integration by parts (first integral) cancels the second term of the second integral:

$$=\frac{(1-K)}{2}\cdot\left(-\frac{1}{2R'_2}\cdot\int_0^\infty e^{-R'_2t}J_{\mathbf{i}}\left(\frac{\gamma h_m}{2}t\right)\cdot\begin{pmatrix}\cos(\Delta t)\\ \mathrm{i}\cdot\sin(\Delta t)\end{pmatrix}_{\mathbf{i}\,\mathrm{odd}}^{\mathbf{i}\,\mathrm{even}}dt\right).$$

Using the previous result for the first part of the A' integral finally gives:

$$\boxed{\begin{aligned}A'_{\mathbf{i}}(\Delta) &= -\tfrac{\mathbf{i}\omega_m}{2}\left(\tfrac{(1+K)}{2}\tfrac{\partial}{\partial\Delta}D_{\mathbf{i}}(\Delta)-\tfrac{(1-K)}{2R_2}A_{\mathbf{i}}(\Delta)\right),\\ K &= (1-S_0)\left(\frac{R_2}{R'_2}\right)^2.\end{aligned}} \tag{A.15}$$

Eq. (A.15) is Eq. (12) in the text.

The dispersion is not exactly analogous to the absorption, because of the opposing symmetry of the trigonometric and Bessel functions in its basic definition (see (A.12) and (A.13) above). Proceeding as with the calculation of A'.

$$D'_{\mathbf{i}}(\Delta) = -\mathbf{i}\cdot(\mathrm{i})^{\mathbf{i}}\cdot\omega_m\cdot\int_0^\infty\int_0^\infty e^{-R'_2(t_1+t_2)} \times\left(\frac{(1+K)}{2}\left(\frac{t_2}{t_1+t_2}\right)J_{\mathbf{i}}\left(\frac{\gamma h_m}{2}(t_1+t_2)\right)\cdot\begin{pmatrix}\sin(\Delta(t_1+t_2))\\ -\mathrm{i}\cdot\cos(\Delta(t_1+t_2))\end{pmatrix}_{\mathbf{i}\,\mathrm{odd}}^{\mathbf{i}\,\mathrm{even}}+\frac{(1-K)}{2}\left(\frac{t_2}{t_1-t_2}\right)\times J_{\mathbf{i}}\left(\frac{\gamma h_m}{2}(t_1-t_2)\right)\cdot\begin{pmatrix}\sin(\Delta(t_1-t_2))\\ -\mathrm{i}\cdot\cos(\Delta(t_1-t_2))\end{pmatrix}_{\mathbf{i}\,\mathrm{odd}}^{\mathbf{i}\,\mathrm{even}}\right)dt_1\,dt_2.$$

The first term follows from the previous calculation without saturation. Change of integration variables in the second term gives:

$$\frac{(1-K)}{2}\cdot\int_0^\infty t_2e^{-2R'_2t_2}\int_{-t_2}^\infty e^{-R'_2t}\frac{1}{t}J_{\mathbf{i}}\left(\frac{\gamma h_m}{2}t\right)\cdot\begin{pmatrix}\sin(\Delta t)\\ -\mathrm{i}\cdot\cos(\Delta t)\end{pmatrix}_{\mathbf{i}\,\mathrm{odd}}^{\mathbf{i}\,\mathrm{even}}dt\,dt_2 =\frac{(1-K)}{2}\cdot\int_0^\infty t_2e^{-2R'_2t_2}\int_{-\infty}^{t_2}e^{-R'_2t}\frac{1}{t}J_{\mathbf{i}}\left(\frac{\gamma h_m}{2}t\right)\cdot\begin{pmatrix}\sin(\Delta t)\\ -\mathrm{i}\cdot\cos(\Delta t)\end{pmatrix}_{\mathbf{i}\,\mathrm{odd}}^{\mathbf{i}\,\mathrm{even}}dt\,dt_2. \tag{A.16}$$

Note the difference between (A.14) and (A.16). The symmetry under sign change of the t integrand is different.Integrating (A.16) by parts:

$$= \frac{(1-K)}{2}\cdot\left(\frac{1}{(2R_2')^2}\int_{-\infty}^{0} e^{+R_2' t}\frac{1}{t}J_{\mathbf{i}}\left(\frac{\gamma h_m}{2}t\right)\cdot\begin{pmatrix}\sin(\Delta t)\\ -i\cdot\cos(\Delta t)\end{pmatrix}_{\mathbf{i}\,\mathrm{odd}}^{\mathbf{i}\,\mathrm{even}} dt - \int_0^{\infty}\left(\frac{te^{-2R_2' t}}{-2R_2'} - \frac{e^{-2R_2' t}}{(2R_2')^2}\right)\times e^{+R_2' t}\frac{1}{t}J_{\mathbf{i}}\left(\frac{\gamma h_m}{2}t\right)\cdot\begin{pmatrix}\sin(\Delta t)\\ -i\cdot\cos(\Delta t)\end{pmatrix}_{\mathbf{i}\,\mathrm{odd}}^{\mathbf{i}\,\mathrm{even}} dt\right).$$

There is no cross-cancellation of terms, as in the derivation of (A.15):

$$= \frac{(1-K)}{2}\cdot\left(\frac{2}{(2R_2')^2}\cdot\int_0^{\infty} e^{-R_2' t}\cdot\frac{1}{t}\cdot J_{\mathbf{i}}\left(\frac{\gamma h_m}{2}t\right)\cdot\begin{pmatrix}\sin(\Delta t)\\ -i\cdot\cos(\Delta t)\end{pmatrix}_{\mathbf{i}\,\mathrm{odd}}^{\mathbf{i}\,\mathrm{even}} dt + \frac{1}{2R_2'}\cdot\int_0^{\infty} e^{-R_2' t}J_{\mathbf{i}}\left(\frac{\gamma h_m}{2}t\right)\cdot\begin{pmatrix}\sin(\Delta t)\\ -i\cdot\cos(\Delta t)\end{pmatrix}_{\mathbf{i}\,\mathrm{odd}}^{\mathbf{i}\,\mathrm{even}} dt\right).$$

This contains now a component that behaves as the integral of an absorption signal. Using the definitions of the basic signals the final answer may be expressed as:

$$D_{\mathbf{i}}'(\Delta) = \frac{i\omega_m}{2}\left(\frac{(1+K)}{2}\left(\left(\frac{R_2'}{R_2}\right)^2\frac{\partial}{\partial\Delta}A_{\mathbf{i}}(\Delta)\right) - \frac{(1-K)}{2}\left(\frac{1}{R_2}D_{\mathbf{i}}(\Delta) + \frac{1}{(R_2)^2}\int_{-\infty}^{\Delta}A_{\mathbf{i}}(\Delta)\,d\Delta\right)\right), \tag{A.17}$$

where $K(1-S_0)(\frac{R_2}{R_2'})^2$, as above.

The recurrence formula for Bessel functions [15] can be used to re-write the integral contribution in (A.17) in terms of $\mathbf{i}\pm 1$ harmonic absorption.

$$D_{\mathbf{i}}'(\Delta) = \frac{i\omega_m}{2}\left(\frac{(1+K)}{2}\left(\left(\frac{R_2'}{R_2}\right)^2\frac{\partial}{\partial\Delta}A_{\mathbf{i}}(\Delta)\right) - \frac{(1-K)}{2}\left(\frac{1}{R_2}D_{\mathbf{i}}(\Delta) + \frac{1}{(R_2)^2}\cdot\frac{\gamma h_m}{2\cdot\mathbf{i}}\cdot(-A_{i+1}(\Delta) + A_{i-1}(\Delta))\right)\right). \tag{A.18}$$

Eqs. (A.17) and (A.18) are Eq. (13) in the text.

References

[1] M. Weger, Passage effects in paramagnetic resonance experiments, Bell Syst. Techn. J. 39 (1960) 1013.

[2] D. Hessinger, C. Bauer, M. Hubrich, G. Jeschke, H.-W. Spiess, Magic-angle sample spinning electron paramagnetic resonance—instrumentation, performance, and limitations, J. Magn. Reson. 147 (2000) 217–225.

[3] L.R. Dalton, B.H. Robinson, L.A. Dalton, P. Coffey, in: J.S. Waugh (Ed.), Advances in Magnetic Resonance, vol. 8, Academic Press, New York, 1976, pp. 149–259.

[4] N.B. Galloway, L.R. Dalton, Approximate methods for the fast computation of EPR and ST-EPR spectra. I. A perturbation approach, Chem. Phys. 30 (1978) 445–459.

[5] B.H. Robinson, Effects of over-modulation on saturation transfer EPR signals, J. Chem. Phys. 78 (1983) 2268–2273.

[6] D.D. Thomas, L.R. Dalton, J.S. Hyde, Rotational diffusion studied by passage saturation transfer electron paramagnetic resonance, J. Chem. Phys. 65 (1976) 3006–3024.

[7] D.D. Thomas, H.M. McConnell, Calculation of paramagnetic resonance spectra sensitive to very slow motion, Chem. Phys. Lett. 25 (1974) 470–475.

[8] E.J. Hustedt, A.H. Beth, Analysis of saturation transfer electron paramagnetic resonance spectra of spin-labeled integral membrane protein, band 3, in terms of the uniaxial rotation diffusion model, Biophys. J. 69 (1995) 1409–1423.

[9] B.H. Robinson, C. Mailer, A.W. Reese, Linewidth analysis of spin labels in liquids. I. Theory and data analysis, J. Magn. Reson. 138 (1999) 199–209.

[10] D.J. Singel, E.D. Walter, S.J. McIlwain, D.A. Schwartz, Passages, 44th Rocky Mountain Conference on Analytical Chemistry, Denver, Poster 98, 2002.

[11] M. Kalin, I. Gromov, A. Schweiger, The continuous wave electron paramagnetic resonance experiment revisited, J. Magn. Reson. 160 (2003) 166–182.

[12] J.S. Hyde, M. Pasenkiewicz-Gierula, A. Jesmanowicz, W.E. Anthroline, Pseudo field modulation in EPR spectroscopy, Appl. Magn. Reson. 1 (1990) 483–496.

[13] W.A. van der Donk, J. Stubbe, G.J. Gerfen, B.F. Bellew, R.G. Griffin, EPR investigation of the inactivation of *E. coli* ribonucleotide reductase with 2′-azido-2′-deoxyuridine 5′-diphophate: evidence for the involvement of the thiyl radical of C225-R1, J. Am. Chem. Soc. 117 (1995) 8908–8916.

[14] G. Folland, Fourier Analysis and its Applications, Wadsworth and Brooks/Cole Advanced Books, Pacific Grove, CA, 1992.

[15] G.N. Watson, A Treatise on the Theory of Bessel Functions, University Press, Cambridge, 1952.

[16] R.D. Nielsen, B.H. Robinson, The effect of field modulation on a simple resonance line shape, concepts in magnetic resonance, Con. Mag. Reson. (2004), in press.

[17] M.K. Bowman, H. Hase, L. Kevan, Saturation behavior of inhomogeneoulsy broadened EPR lines detected with magnetic field modulation, J. Magn. Reson. 22 (1976) 23–32.

[18] I.S. Gradshteyn, I.M. Ryzhik, Table of Integrals, Series, and Products, Academic Press, New York, 1980.

[19] Mathlab ver. 6.1 (2001) Mathworks, Cambridge, MA, http://www.mathworks.com.

[20] T.M. Okonogi, A.W. Reese, S.C. Alley, P.B. Hopkins, B.H. Robinson, Flexibility of duplex DNA on the submicrosecond timescale, Biophys. J. 77 (1999) 3256–3276.

[21] E.J. Hustedt, C.E. Cobb, A.H. Beth, J.M. Beechem, Measurement of rotational dynamics by simultaneous nonlinear analysis of optical and EPR data, Biophys. J. 64 (1993) 614–621.

[22] W.H. Press, Numerical Recipes: The Art of Scientific Computing, Cambridge University Press, New York, 1989.

[23] A.H. Beth, R.C. Perkins, S.D. Venktaramu, D.E. Pearson, C.R. Park, J.H. Park, L.R. Dalton, Advantages of deuterium modification of nitroxide spin labels for biological EPR studies, Chem. Phys. Lett. 69 (1980) 24–28.

[24] D.K. Faddeev, V.N. Faddeeva, Computational Methods of Linear Algebra, W.H. Freeman, San Francisco, 1963.